ACS APPLIED MATERIALS & INTERFACES

Spotlight on Applications

www.acsami.org

Comparative Study of Potential Applications of Graphene, MoS_2, and Other Two-Dimensional Materials in Energy Devices, Sensors, and Related Areas

C. N. R. Rao,* K. Gopalakrishnan, and Urmimala Maitra

Chemistry and Physics of Materials Unit, New Chemistry Unit, International Centre for Materials Science, CSIR Centre of Excellence in Chemistry and Sheik Saqr Laboratory, Jawaharlal Nehru Centre for Advanced Scientific Research, Jakkur, Bangalore 560064, India

ABSTRACT: Novel properties of graphene have been well documented, whereas the importance of nanosheets of MoS_2 and other chalcogenides is increasingly being recognized over the last two to three years. Borocarbonitrides, $B_xC_yN_z$, with insulating BN and conducting graphene on either side are new materials whose properties have been attracting attention. These two-dimensional (2D) materials contain certain common features. Thus, graphene, MoS_2, and borocarbonitrides have all been used in supercapacitor applications, oxygen reduction reactions (ORRs), and lithium-ion batteries. It is instructive, therefore, to make a comparative study of some of the important properties of these layered materials. In this article, we discuss properties related to energy devices at length. We examine the hydrogen evolution reaction facilitated by graphene, MoS_2, and related materials. We also discuss gas and radiation sensors based on graphene and MoS_2 as well as gas storage properties of graphene and borocarbonitrides. The article should be useful in making a judicious choice of which 2D material to use for a particular application.

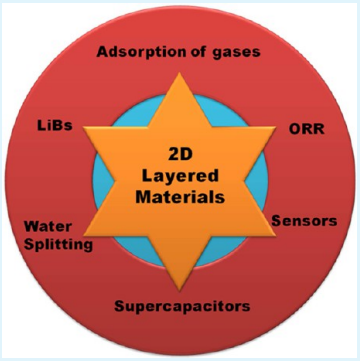

KEYWORDS: *Graphene, MoS_2, borocarbonitrides, 2D materials, supercapacitors, lithium batteries*

1. INTRODUCTION

The discovery of graphene and its fascinating properties[1−4] has stimulated serious research on other layered materials. Thus, in the last three to four years, MoS_2 and other layered transition metal dichalcogenides (TMDs) have been the subject of intense investigation.[5−9] Single- and few-layered MoS_2 exhibits novel properties that are distinctly different from those of graphene.[10] Whereas graphene is a gapless material, the stable 2H form of single-layered MoS_2 is a direct band gap semiconductor.[11] Some properties of single-layer MoS_2 (2H) arise from valley polarization arising from spin−orbit splitting and transformation of the 2H form to the 1T form with entirely different properties.[12] Properties of graphene and related two-dimensional (2D) materials have been exploited for applications in energy devices, such as supercapacitors and Li-ion batteries, as well as the oxygen reduction reaction (ORR) of fuel cells. Another interesting material that has been added to the family of layered materials over the past few years is borocarbonitrides with the formula $B_xC_yN_z$.[13] Borocarbonitrides, with insulating BN on one side and conducting graphene on the other, exhibit interesting properties. Though homogeneous compositions of borocarbonitrides have not been achieved, the materials have still been applied in supercapacitors, Li-batteries, and ORRs. They possess high surface areas, just like graphene, and show useful gas adsorption properties.

In this article, we discuss the performance of energy devices based on graphene and graphene analogues of inorganic materials, such as MoS_2 and $B_xC_yN_z$. In addition, we compare gas adsorption properties of graphene and $B_xC_yN_z$ for environmentally important gases like CO_2 and CH_4. Another topic of importance related to energy is the hydrogen evolution reaction (HER). A comparative study of graphene and layered MoS_2 in photocatalytic and electrochemical HER is presented. We also present a comparison of the performance of graphene- and MoS_2-based radiation and chemical sensors. We believe that the comparative study of the properties and potential applications of graphene, MoS_2, and borocarbonitrides, particularly those related to energy devices, will be valuable to the research community.

2. GAS ADSORPTION AND STORAGE

Gas storage is of great relevance to energy as well as environmental needs. Single-layer graphene is theoretically predicted to possess a large surface area of 2600 m^2/g.[14] The surface areas of few-layer graphenes are also quite large, being on the order of 270−1550 m^2/g.[15,16] Graphene has been found to be an ideal material for adsorption and storage of various gases, surpassing carbon nanotubes. Theoretical calculations[17] suggest that the H_2 adsorption capacity of graphene can approach values of ∼6 wt % and 62 kg of H_2 per m^3, a value comparable to that set by the US Department of Energy (DOE) for on-board hydrogen storage for transportation applications. Experimental H_2 adsorption studies on thermally exfoliated and other few-layer graphene samples by Ghosh et

Received: December 25, 2014
Accepted: March 30, 2015
Published: March 30, 2015

DOI: 10.1021/am509096x
ACS Appl. Mater. Interfaces 2015, 7, 7809−7832

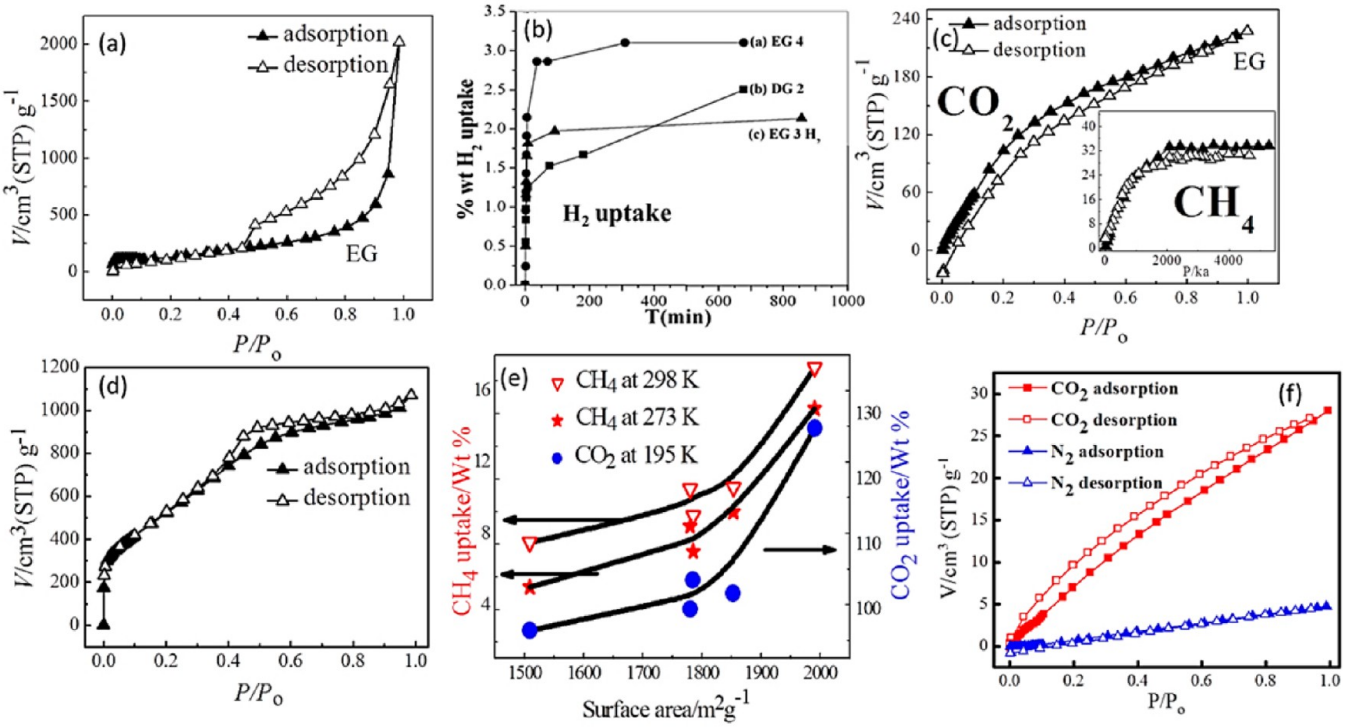

Figure 1. Surface area and gas adsorption properties for (a) N_2 adsorption−desorption isotherms of EG, (b) wt % of H_2 uptake by graphene (EG3 and EG4 are EG samples with different surface areas, and DG is the graphene obtained from the transformation of nanodiamond), (c) CO_2 and CH_4 adsorption−desorption isotherms of EG, (d) N_2 adsorption−desorption isotherms of $BC_{1.9}N$. Reprinted with permission from ref 13 (Copyright 2013 The Royal Society of Chemistry). (e) Variation of CO_2 and CH_4 uptake in $B_xC_yN_z$ with surface area. Reprinted with permission from ref 16 (Copyright 2008 American Chemical Society). (f) Selectivity for CO_2 adsorption relative to N_2 by $BC_{1.9}N$. Reprinted with permission from ref 30 (Copyright 2010 WILEY-VCH Verlag GmbH & Co. KGaA, Weinheim).

al.[16] have shown a H_2 uptake of 1.7 wt % at atmospheric pressure and 77 K. A maximum adsorption of 3 wt % was achieved at 298 K and 100 atm for thermally exfoliated graphene (EG). Figure 1(a,b) shows N_2 and H_2 adsorption isotherms of thermally exfoliated graphene (EG). Reduced graphene oxide (RGO) with a surface area of 640 m^2/g showed H_2 adsorption capacities of 1.2 and 0.1 wt % at 77 and 298 K, respectively, at atmospheric pressure.[18] Introduction of cross-linkers in between graphene sheets leads to an increase in the H_2 uptake capacity of few-layer graphene.[19] Porous graphene frameworks pillared by organic linkers (~800 m^2/g Brunauer−Emmett−Teller (BET) surface area), however, show adsorption of 1 wt % H_2 at 1 atm and 77 K.[20] Ab initio calculations on H_2 storage capacity of carbon nanoscrolls intercalated with alkali metals predict an adsorption capacity of 3 wt %.[21]

The interaction energy between graphene and H_2 plays a significant role in determining the capacity for H_2 storage. The strength of chemisorption of hydrogen on single-wall nanotubes was calculated to be ~2.5 eV per H atom, whereas that of physisorption is 0.11 eV per H_2 molecule.[22] Hydrogenation of graphene would therefore be expected to provide the possibility of greater % storage of H_2 in graphene. Several methods have been adapted for hydrogenation of graphene, including hydrogen plasma[23−26] and catalytic hydrogenation,[27] yielding a maximum storage of 1.25−1.78 wt %. Birch reduction of various few-layer graphene samples has been carried out by Subrahmanyam et al.[28] Elemental analysis of the hydrogenated graphene samples shows the hydrogen content to be ~5 wt %. It was possible to recover almost all of the H_2 by heating the Birch-reduced graphene to 500 °C or by irradiating the sample with UV light or a KrF excimer laser. Birch reduction of graphene nanoribbons of graphene showed a H_2 uptake of 3 wt %.

Few-layer graphenes show good adsorption of green-house gases like CO_2 and CH_4.[29] EG and RGO samples with oxygen functionalities on the surface show an uptake of CO_2 of ~51 wt % at 298 K and 50 bar (see Figure 1(c)). This is lower than that of activated charcoal, which shows 64 wt % uptake of CO_2 at 195 K and 1 atm. Activated charcoal has both high surface area and a large density of oxygen functional groups on the surface. Porous graphene frameworks pillared by organic linkers show 60−110 wt % of CO_2 at 195 K and 0.85 atm and ~40 wt % at 273 K and high pressure.[20] Uptake of CH_4 by graphene samples varies between 0 and 3 wt % at 273 K and 5 MPa depending on the surface area of different graphene samples.

High surface area borocarbonitrides ($B_xC_yN_z$) prepared from activated charcoal by reaction with boric acid and urea have been explored for adsorption of CO_2 and methane.[13,30] Borocarbonitrides with surface areas ranging from 1509 m^2/g to 1990 m^2/g showed remarkable CO_2 uptake of 64 and 128 wt % at 300 K (50 bar) and 195 K (1 atm), respectively (see Figure 1(d,e)). CH_4 uptake is ~17 wt % at 273 K and 5 MPa. First-principles calculations indicate the presence of strongly adsorbing sites for CH_4 and CO_2 on $B_xC_yN_z$, leading to such high adsorption properties. Borocarbonitrides also show selectivity of CO_2 over N_2 of ~10 wt % at 293 K and 1 atm as demonstrated in Figure 1(f). It appears high surface area borocarbonitrides, which are inexpensive materials, may be useful in CO_2 sequestration and related applications.

DOI: 10.1021/am509096x
ACS Appl. Mater. Interfaces 2015, 7, 7809−7832

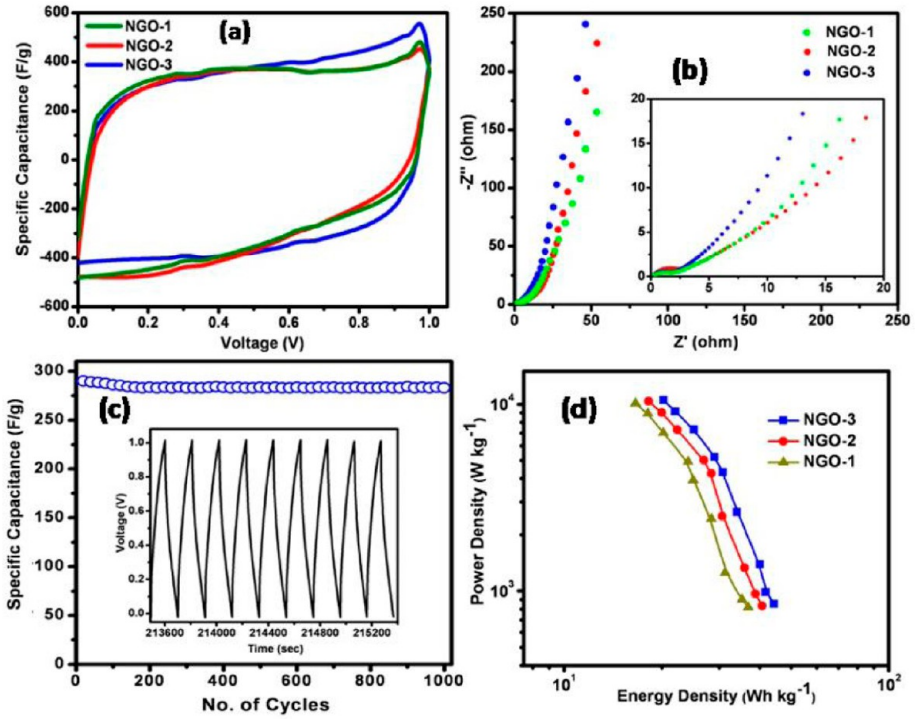

Figure 2. (a) Cyclic voltammograms of NGOs at a scan rate of 20 mV/s. (b) Nyquist curves for NGO electrodes. (c) Specific capacitance versus cycle number of NGO-3 measured at a current density of 0.5 A/g within an operational window of 0.0−1 V (inset shows charge−discharge curves of the last few cycles for NGO-3). (d) Ragone plots of-NGO based supercapacitors. Reprinted with permission from ref 51 (Copyright 2013 The Royal Society of Chemistry).

3. SUPERCAPACITORS

Electrochemical supercapacitors are passive, static electrical energy storage devices that store a large amount of energy relative to conventional capacitors but less than that of batteries. They are similar to conventional capacitors except that the metal electrodes are replaced by a highly porous electrode. On the basis of their energy storage mechanism, supercapacitors can be classified into two types.[31] One is the electrical double layer capacitor (EDLC), where the charge storage mechanism is non-Faradaic and no charge transfer occurs during charging and discharging across the electrode−electrolyte interface, and the energy storage is electrostatic. The second type of supercapacitor is the pseudocapacitor, which has fast and reversible charge-transfer reactions between the electrode surface and the electrolyte ions; these processes are Faradaic. These two mechanisms can function simultaneously depending on the nature of the electrode material. Of the many materials reported in the literature, porous carbons, such as activated carbon, carbon nanotubes, and graphene, show phenomenal supercapacitor performance.[32,33] Inorganic analogues of graphene (e.g., MoS_2) also show promising electrochemical properties.[12]

Among the few-layer graphenes, EG shows a specific capacitance of 117 F/g in 1 M H_2SO_4. In an ionic liquid, it shows a specific capacitance of 75 F/g with a maximum energy density of 31.9 Wh/kg in a two-electrode system. Ruoff et al.[34] have used chemically modified graphene (RGO) with a surface area of 705 m^2/g to obtain specific capacitances of 135 and 99 F/g in aqueous (5.5 M KOH) and organic ($TEABF_4$) electrolytes, respectively. Graphene prepared from gas phase hydrazine reduction of graphene oxide shows a maximum specific capacitance of 205 F/g with a power density of 10 kW/kg at an energy density of 28.5 Wh/kg in an aqueous electrolyte.[35] Microwave exfoliated graphite oxide (MEGO) gives a specific capacitance as high as 191 F/g in KOH with a large surface area (463 m^2/g).[36] When chemically activated, the surface area of MEGO (a-MEGO) goes up to ~2400 m^2/g with high electrical conductivity and low oxygen and hydrogen content.[37] Conventional supercapacitors based on curved graphene in an ionic liquid typically show 100−250 F/g at a high current density of 1 A/g with a discharge voltage of 4.0 V and exhibit an energy density of 85.6 Wh/kg.[38] Bando et al.[39] have employed the sugar-blowing technique to grow a three-dimensional (3D) self-supported graphene product, called strutted graphene (SG). With a two-electrode system, the capacitance in H_2SO_4 solution was 250 F/g at 1 A/g, which slowly decreased to 130 F/g at a high current of 100 A/g. SG-based supercapacitors show high power density of 893 kW/g at 100 A/g. Solvothermal reduction of a graphene oxide (GO) dispersion in propylene carbonate (PC) yields a self-assembled graphene organogel (SGO).[40] A supercapacitor based on SGO with PC exhibits a specific capacitance of 140 F/g at 1 A/g with the maximum energy density being 43.5 Wh/kg. Graphene synthesized by the reduction of dry ice in magnesium and calcium metal flames shows a specific capacitance of 220 F/g at a current density of 0.1 A/g in 6 M KOH electrolyte.[41] NiO-deposited 3D graphene networks exhibited a high specific capacitance of ~816 F/g at a scan rate of 5 mV/s and a good cycling performance in 3 M KOH.[42]

Three-dimensional, shape-engineered graphene hydrogels synthesized using a simple gelation process have been used for high rate, large capacity supercapacitor electrodes.[43] The surface area of the graphitic gel is measured to be 615 m^2/g with an areal capacitance of 33.8 mF/cm^2 at 1 mA/cm^2. An activated carbon aerogel containing graphene (ACAG) with a

DOI: 10.1021/am509096x
ACS Appl. Mater. Interfaces 2015, 7, 7809−7832

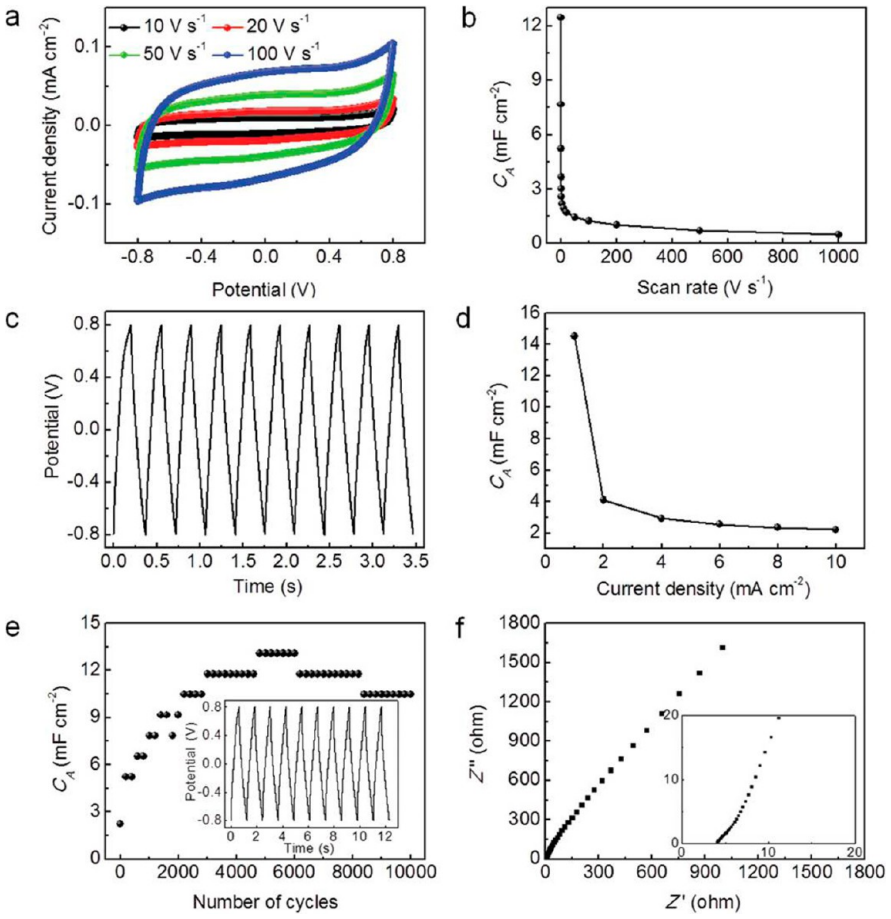

Figure 3. Electrochemical energy-storage performance of the edge-oriented MoS_2 films. (a) CV curves performed over a potential window between −0.8 and 0.8 V at scan rates of 10, 20, 50, and 100 mV/s. (b) Variation of areal capacitance at different scan rates. (c) Discharge/charge profiles obtained at a current density from 10 mA/cm^2 (the current density is the applied current divided by the geometrical area of the electrode: 0.785/cm^2). (d) Variation of areal capacitance at different current densities from 1 to 10 mA/cm^2. (e) 10000 cycling tests measured at 10 mA/cm^2. Inset shows the discharge/charge profiles obtained after 10000 cycling tests at a current density of 10 mA/cm. (f) EIS of the flexible device with an enlarged high frequency region in the inset. Reprinted with permission from ref 59 (Copyright 2014 WILEY-VCH Verlag GmbH & Co. KGaA, Weinheim).

surface area of 1384 m^2/g has been employed as a supercapacitor electrode.[44] The capacitance value of ACAG (300 F/g) is better than that of activated carbon (189 F/g) at 1 A/g in aqueous KOH. Holey graphene prepared by ultrarapid heating during the exfoliation of graphite oxide shows an excellent capacitance of 170 F/g at 50 A/g in 6 M KOH.[45] Graphene modified by 6-amino-4-hydroxy-2-naphthalenesulfonic acid (ANS) shows a specific capacitance that is higher than that of the pristine sample.[46] The π-electrons and amine ($-NH_2$) functional groups in ANS interact with graphene through $\pi-\pi$ and covalent bonding. Hydroxyl and sulfonic acid groups increase the hydrophilicity and dispersion stability of ANS-modified graphene and thus increase the capacitance. ANS-modified graphene exhibits a specific capacitance of 375 F/g at a current density of 1.3 A/g and good electrochemical cyclic stability. The supercapacitor performance of graphene depends on the electrolyte used for measurements. Xue et al.[47] tested the supercapacitor performance of graphene in four different nonaqueous electrolytes. The performance and specific capacitance vary in the order of $P_{4,4,4,4}$ BF_4/acetonitrile (~78 F/g) < BMIM BF_4/acetonitrile (~75 F/g) = BPy BF_4/acetonitrile (~73F/g) < Et_4N BF_4/acetonitrile (~70F/g) at a current density of 1 A/g. Of these, Et_4N BF_4 showed better performance, including a long duration time, excellent rate performance, and a small IR drop. The improved performance is understood in terms of the relative ionic sizes of the electrolyte Et_4N^+ (3.43 Å), BPy^+ (3.51 Å), $BMIM^+$ (3.56 Å), and $P_{4,4,4,4}{}^+$ (4.45 Å), which lead to different conductivities and charge densities at the electrode−electrolyte interlayer.

Doped graphenes show enhanced supercapacitor performance because doping helps to manipulate its electronic structure in a desirable fashion.[48] A change in the electronic structure of graphene allows enhanced binding of ions in solution. Zhao et al.[49] prepared nitrogen-doped graphene by the reduction of graphene oxide with urea and obtained a specific capacitance of 255 F/g at 0.5 A/g in an aqueous electrolyte (6 M KOH). An increase in the nitrogen content in graphene increases the specific capacitance,[50] and with a nitrogen content varying in the 2−8 wt % range, a specific capacitance of 126 F/g at 5 mV/s is found in an aqueous electrolyte. Graphene oxide doped with nitrogen prepared under microwave irradiation using urea as the nitrogen source and containing 18 wt % of nitrogen exhibits a specific capacitance of 465 F/g at 5 mV/s in an aqueous electrolyte.[51] Typical cyclic voltammograms (CV), Nyquist plots, cyclic stability, and Ragone plots of these samples are shown in Figure 2(a and b). Cyclic stability was excellent with capacitance retention of 97% after 1000 cycles at 0.5 A/g (see Figure 2(c)). The energy density is 44.4 Wh/kg

DOI: 10.1021/am509096x
ACS Appl. Mater. Interfaces 2015, 7, 7809−7832

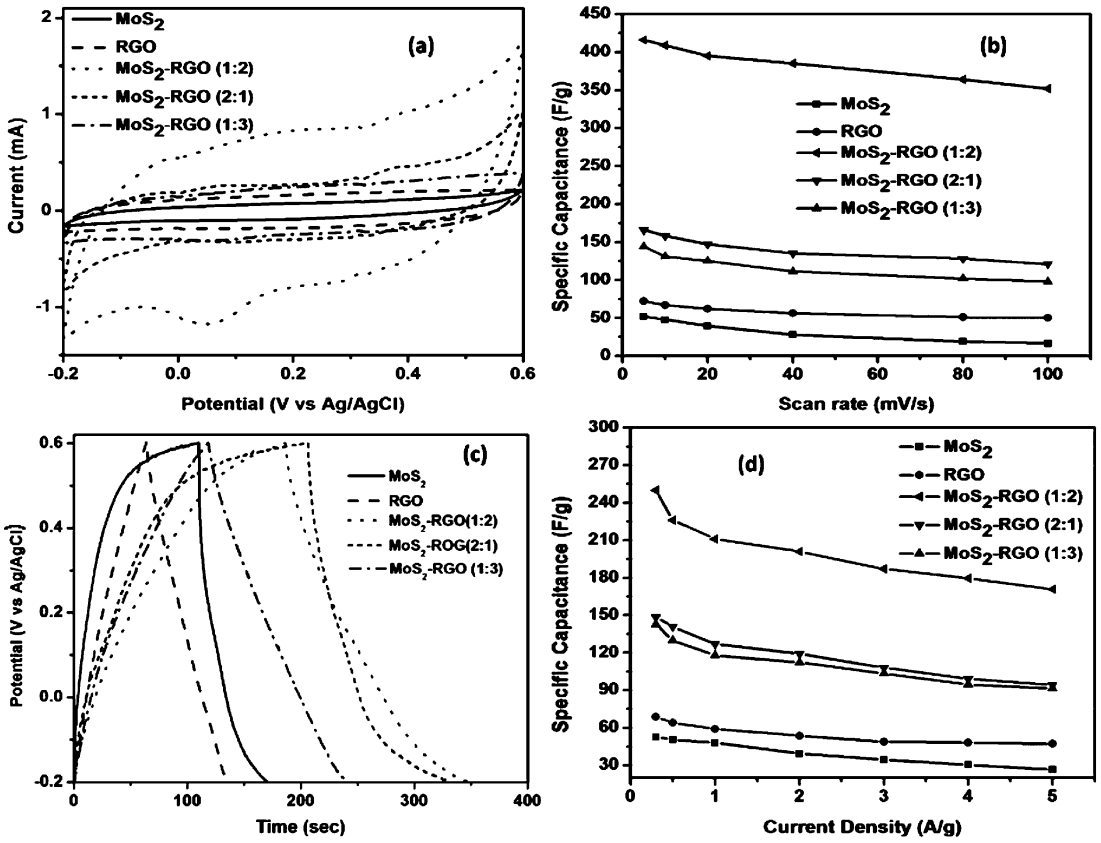

Figure 4. (a) Cyclic voltammograms of MoS_2, RGO, and MoS_2/RGO nanocomposites at 100 mV/s. (b) Specific capacitance of MoS_2, RGO, and MoS_2/RGO nanocomposites at different scan rates. (c) Galvanostatic charge−discharge curves of MoS_2, RGO, and MoS_2/RGO nanocomposites at a current density of 1 A/g. (d) Specific capacitance of MoS_2, RGO, and MoS_2/RGO nanocomposites at different current densities. Reprinted with permission from ref 67 (Copyright 2014 Institution of Civil Engineers Publishing).

(two-electrode) at a current density of 0.3 A/g, whereas the power density is 852 W/kg (Figure 2(d)). Nitrogen doping produces different types of nitrogen in the graphene structure.[51] Of these, pyrrolic and pyridinic nitrogens are most favorable for good supercapacitor performance. Sun et al.[52] suggest that electrochemically active nitrogen atoms (pyrrolic and pyridinic nitrogens) control the electronic structure and the accommodation of K^+ ions on the electrode surface. Water molecules around the K^+ ions near the electrode surface produce redox reactions between water and the electrochemically active functional groups. Graphitic nitrogen increases the conductivity of the graphene electrode and allows the transport of electrons, thereby enhancing the capacitance.

Boron-doped graphene (BG) made by the fried ice method gives a specific capacitance of 281 F/g in an aqueous electrolyte medium (2 M H_2SO_4).[53] BG prepared by a simple pyrolysis process using GO and boric acid shows a specific capacitance of 172.5 F/g at 0.5 A/g and maintains 96.5% of the initial capacity after continuous cycling 5000 times.[54] Boron doping increases the capacitance by ∼80% compared to pristine graphene. High surface-area borocarbonitrides prepared by the urea route have been examined for supercapacitor applications.[50] $BC_{4.5}N$ shows a specific capacitance of 178 F/g in an aqueous electrolyte. In an ionic liquid, the specific capacitance value of $BC_{4.5}N$ is 240 F/g. In an aqueous medium, $BC_{4.5}N$ exhibits supercapacitor characteristics superior to those of nitrogen-doped graphene or reduced graphene oxide.

Two-dimensional semiconducting materials like MoS_2 and WS_2 have layered structures similar to graphene.[12] MoS_2 has attracted more attention for use in supercapacitors because of its higher intrinsic ionic conductivity and theoretical capacity. Because of its layered structure consisting of covalently bound S−Mo−S trilayers held by van der Waals forces, this material was considered to be a suitable alternative to graphene. Soon et al.[55] reported the presence of double layer charge behavior in MoS_2 nanowall films at alternating current frequencies up to 100 Hz. Supercapacitor performance of MoS_2 is comparable to that of carbon nanotube arrays. Ajayan et al.[56] reported a MoS_2-based microsupercapacitor with a capacitance of 8 mF/cm^2 (volumetric capacitance of 178 F/cm^3) and excellent cyclic performance through a simple and low-cost spray painting on Si/SiO_2 chip followed by laser patterning. Kim and co-workers[57] have synthesized MoS_2 nanostructures through a one-pot hydrothermal method and showed a specific capacity of ∼92 F/g at a current density of 0.5 mA/cm^2 in 1 M Na_2SO_4 aqueous electrolyte. Flower-like MoS_2 nanospheres prepared by the hydrothermal route exhibit a specific capacitance of 122 F/g at 1 A/g in 1 M KCl elctrolyte.[58]

Edge-oriented MoS_2 nanoporous films synthesized by electrochemical anodization of molybdenum metal in the presence of sulfur vapor show good supercapacitor performance.[59] CVs were recorded on the flexible device to access the electrochemical charge storage behavior of the edge-oriented MoS_2 thin-film (Figure 3(a)). A capacitance up to 12.5 mF/cm^2 was obtained from cyclic voltammogram measurements at a scan rate of 50 mV/s (Figure 3(b)) and 14.5 mF/cm^2 from galvanostatic charge−discharge measurements at a current density of 1 mA/cm^2 (Figure 3(c and d)). These MoS_2 films

DOI: 10.1021/am509096x
ACS Appl. Mater. Interfaces 2015, 7, 7809−7832

Table 1. Supercapacitor Performance of Graphene, MoS_2, and Borocarbonitrides

materials	preparation method	C_{sp} (CD) (F/g)	electrolyte	energy density (Wh/kg)	ref
		Graphene			
EG	thermal exfoliation	115 (5 A/g)	H_2SO_4 $PYR_{14}TFSI$	31.9	70
chemically modified graphene	chemical reduction	135 (10 mA)	5.5 M KOH $TEABF_4$		34
curved graphene	chemical method	100−250 (1A/g)	$EMIMBF_4$	85.6	38
microwave exfoliated graphene	microwave	191 (1A/g)	5 M KOH		36
chemically activated graphene	thermal	166 (5.7 A/g)	BMIM BF_4	∼70	37
strutted graphene	thermal	250 (1A/g)	H_2SO_4		39
activated carbon aerogel graphene	thermal	300 (1A/g)	6 M KOH		44
self-assembled graphene organogel	solvothermal	140 (1A/g)	$TEABF_4$	43.5	40
dry-ice reduced graphene	solvothermal	220 (0.1A/g)	6 M KOH		41
RGO-activated carbon	thermal	133.3 (2A/g)	TEA BF_4	43.6	71
graphene/carbon nanotube foam	solvothermal	286 (1.7 mA/cm^2)	6 M KOH	39.7	72
chemically bonded GO/CNT	solvothermal	110 (1A/g)	TEA BF_4	34.3	73
GO-carbon nanotube	solvothermal	326	6 M KOH	21.7	74
GO-carbon nanotube	solvothermal	201 (0.5A/g)	TEA BF_4	155.6	75
nitrogen-doped graphene	hydrothermal	255 (0.5 A/g)	6 M KOH		49
	hydrothermal	326 (0.2 A/g)	6 M KOH	25.02	52
	hydrothermal	308 (3 A/g)	6 M KOH		76
	hydrothermal	194 (10 mV/s)	1 M KCl		77
	thermal	249 (3 A/g)	1 M $TEABF_4$	34.5	78
	microwave	320 (0.3 A/g	6 M KOH	44.4	51
	plasma-CVD	282 (1 A/g)	1 M $TEABF_4$	∼48	79
	plasma-CVD	9.5 mF/cm^2	1 M H_2SO_4		80
	thermal	245.9 (1 A/g)	1 M $TBABF_4$		81
	thermal	138.1 (1 A/g)	1 M $TEABF_4$	80.5	82
	thermal	188 (5 mV/s)	25% KOH	2.24	83
	solvothermal	242(1 A/g)	1 M H_2SO_4	8.4	84
$B_xC_yN_z$	thermal	172 F/g, 240 F/g	1 M H_2SO_4, 1 M $TBABF_4$		32
		MoS_2			
MoS_2 nanosheet	hydrothermal	8 mF/cm^2	KOH		56
MoS_2 nanosheet	hydrothermal	92 F/g (0.5 mA/cm^2)	1 M Na_2SO_4		57
MoS_2 nanospheres	hydrothermal	122 F/g (1 A/g)	1 M KCl		58
MoS_2 nanoporous films	electrochemical anodization	14.5 mF/cm^2 (1 mA/cm^{-2})	1 M LiOH		85
mesoporous MoS_2	hydrothermal	403 F/g (1 mV/s)	1 M KCl		60
3D MoS_2	Hydrothermal	168 F/g (1 A/g)	1 M KCl		61
porous tubular C/MoS_2	thermal	210 F/g (1 A/g)	3.0 M KOH		63
MoS_2/graphene	microwave	265 (10 mV/s)	1 M $HClO_4$	63	64
MoS_2/graphene	layer-by-layer	282 F/g (20 mV/s)	1 M Na_2SO_4		65
MoS_2/graphene	solvothermal	243 F/g (1 A/g)	1 M $HClO_4$		66
MoS_2/graphene	hydrothermal	416 F/g (5 mV/s)	1 M H_2SO_4		67
MoS_2/PANI (1:6)	polymerization	567 (0.3 A/g)	2 M H_2SO_4		68

show an increased capacitance from 2.2 to 10.5 mF/cm^2 after 10000 testing cycles at a current density of 10 mA/cm^2 (Figure 3(e)), and the quasitriangular shape did not change significantly (inset of Figure 3e). Electrochemical impedance spectra of MoS_2 films show excellent pseudocapacitive behavior without the appearance of the semicircle related to charge transfer resistance. The equivalent series resistance is ∼4 ohm. The hydrothermally synthesized mesoporous MoS_2 electrode delivers a capacitance of 376 and 403 F/g at a scan rate of 1 mV/s in 1 M Na_2SO_4 and KCl electrolytes, respectively.[60] Three-dimensional flower-like MoS_2 shows a specific capacitance of 168 F/g at a current density of 1 A/g, and it retained 92.6% of capacitance even after 3000 cycles.[61] Fiber-based solid-state supercapacitors of MoS_2,TiS_2,TaS_2, and $NbSe_2$ showed a maximum capacitance of 30 F cm^{-3} (at a current of 0.1 μA).[62]

Porous tubular C/MoS_2 nanocomposites synthesized by reacting glucose and $(NH_4)_2MoS_4$ as carbon and MoS_2 sources, respectively, showed a capacitance of 210 F/g whereas the bulk MoS_2 showed 40 F/g at 1 A/g.[63] MoS_2-graphene composites exhibit a high specific capacitance with good reversibility.[64−67] MoS_2 nanosheets in different proportions deposited on reduced graphene oxide (RGO) by microwave heating show specific capacitance values of 128, 265, and 148 F/g at 10 mV/s, and the energy density is found to be 63 Wh/kg.[64] These composite materials reveal that the charge storage is formed by few-layer MoS_2 covalently attached to the RGO. This indicates that the electrochemical process is entirely controlled by the interaction between the electrolyte and the MoS_2 surface. MoS_2-graphene nanosheets formed by layer-by-layer assembly demonstrate high capacitance and cycle life.[65] MoS_2-graphene nanosheets not only prevent the agglomeration of MoS_2 nanosheets but also restrict the growth of MoS_2 during layer-by-layer by the bond formed between MoS_2 nanosheets and graphene. The hybrid film electrode shows a specific capacitance of 282 F/g at a scan rate of 20 mV/s with improved cycle life retaining over

DOI: 10.1021/am509096x
ACS Appl. Mater. Interfaces 2015, 7, 7809−7832

93% of its initial capacitance. MoS_2-graphene composites synthesized by a modified L-cysteine-assisted solution-phase method shows a capacitance of 243 F/g at a discharge current density of 1 A/g with an energy density of 73.5 Wh/kg at a power density of 19.8 kW/kg.[66]

Rao and co-workers have synthesized MoS_2 and reduced graphene oxide (RGO) composites of different compositions and studied their supercapacitor performances.[67] The best results are obtained with the MoS_2/RGO (1:2) composite as shown in Figure 4. The CV curves for MoS_2/RGO nanocomposites show quasi-rectangular CV curves with small humps due to the redox process. The quasi-rectangular CV curves indicate excellent charge storage capability of the nanocomposites, which resemble those of an ideal supercapacitor, showing a maximum capacitance of 416 F/g with MoS_2/RGO (1:2) at a scan rate of 5 mV/s. It is smaller on either side of this composition, as in the 2:1 and 1:3 composites. When the scan rate increases, the current increases and the capacitance decreases as shown in Figure 4(b). Figure 4(c) shows the charge−discharge curves measured at a current of 1 A/g. The discharge time of MoS_2/RGO (1:2) is significantly longer than the other composites, and the curves look nearly symmetrical, indicating remarkable charge storing ability of this composite. The calculated specific capacitance of this composite is 249 F/g when measured at 0.3 A/g. The specific capacitance of MoS_2, RGO, and MoS_2/RGO composites obtained at different current densities are shown in Figure 4(d). The synergistic effect is calculated to be 118% in the 1:2 composite. The electronic conductivity of RGO and surface properties of both MoS_2 and RGO in the composites appear to be responsible for the good specific capacitance. MoS_2/PANI composites with PANI in different compositions showed excellent supercapacitor performance.[68] The 1:1 and 1:6 MoS_2/PANI composites show capacitance values of 417 and 567 F/g, respectively, with cyclic stability that is better than PANI alone. MoS_2 and polypyrrole nanocomposites prepared by in situ oxidative polymerization showed a specific capacitance of ∼700 F/g at a scan rate of 10 mV/s.[69] The increase in specific capacitance of the nanocomposite is attributed to the small charge transfer resistance as well as the contribution from the MoS_2 monolayer.

In Table 1, we summarize the supercapacitor properties of graphene, MoS_2, $B_xC_yN_z$, and related layered materials. Looking at all of the available data, it appears that heavily nitrogenated graphene oxide[51] and MoS_2/RGO[67] (PANI)[68] composites are good candidates for supercapacitor applications.

4. LITHIUM-ION BATTERIES

Lithium-ion batteries (LIBs) have become predominant in battery technology due to their high energy density, high power density, high reversible capacity, and excellent storage characteristics.[86] Carbon electrodes play an important role in battery performance, and graphene shows a reversible capacity that is larger than that of a commercial anode material (graphite) due to its high surface area, electrical conductivity, and high chemical stability. Ajayan et al.[87] deposited nitrogen-doped graphene on a Cu foil by the CVD process and showed its double reversible discharge capacity. The increase in reversible discharge capacity is ascribed to defects created by nitrogen doping. Figure 5(a) shows the cyclic voltammogram of the N-doped graphene electrode conducted at a scan rate of 0.1 mV/s in 1 M solution of $LiPF_6$. The lithium insertion potential is quite low. Figure 5(b) shows the voltage versus

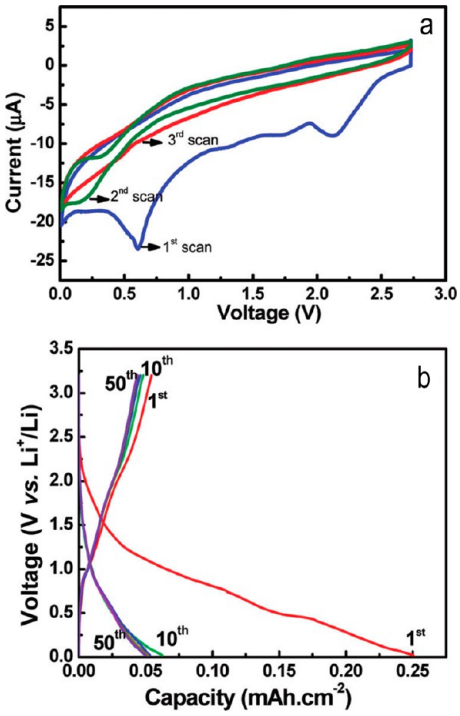

Figure 5. (a) Cyclic voltammograms of N-doped graphene electrode in 1 M solution of $LiPF_6$ in 1:1 (v/v) mixture of ethylene carbonate (EC) and dimethyl carbonate (DMC) as the electrolyte with Li as the counter and reference electrode (scan rate: 0.1 mV/s); (b) Charge−discharge voltage profiles for the N-doped graphene electrode cycled at a rate of 5 A/cm^2 between 3.2 and 0.02 V vs Li/Li$^+$. Reprinted with permission from ref 87 (Copyright 2010 American Chemical Society).

specific capacity plots, and the discharge plateau is attributed to the formation of solid electrolyte interface on the surface of the graphene. N-doped graphene obtained from thermal annealing of GO under ammonia shows an increase in specific capacity with an increase in charge−discharge cycles and superior cyclic stability.[88] N-doped graphene exhibits 452 and 684 mAh/g in the 100th and 501st cycle, respectively, with electrochemical performance that is higher than pristine graphene or commercial graphite. Nitrogen-doped graphene containing ∼3 at. % N exhibits a reversible capacity of 1043 mAh/g in the first cycle and 872 mAh/g in the 30th cycle, which is higher than that of pristine graphene with 955 and 638 mhA/g in the first and 30th cycles, respectively.[89] Nitrogen-doped graphene from glucose synthesized by a sacrificial template produced three different types of nitrogen dopants (pyridinic, pyrrolic, and graphitic nitrogens) in the graphene lattice with a microporous structure and high specific surface area of 504 m^2/g.[90] It shows an enhanced reversible capacity of 832.4 mAh/g at 100 mA/g and an excellent cycling stability of 750.7 mAh/g after 108 discharge−charge cycles. Nitrogen-doped graphene oxide with 2.0 wt % of nitrogen reveals excellent reversible capacity of 600 mAh/g at a current density of 0.1 C (1 C = 372 mA/g) after 60 cycles, which is better than that of pristine RGO (350 mAh/g at a current density of 0.1 C).[91] Hollow microspheres of nitrogen-doped graphene synthesized through the sacrificial template method exhibited an initial discharge capacity of 2716.4 mAh/g, which is significantly higher than the theoretical discharge capacity of graphite.[92]

Borocarbonitrides, which have insulating BN and conducting graphene as limiting compositions, exhibit a remarkably high

DOI: 10.1021/am509096x
ACS Appl. Mater. Interfaces 2015, 7, 7809−7832

lithium cyclability and current rate capability.[93] The borocarbonitrides prepared for this purpose by the high-temperature reaction of carbon, boric acid, and urea possess high surface areas and are likely to contain BCN rings as well as graphene and BN domains. The borocarbonitrides, $B_{0.15}C_{0.73}N_{0.12}$, with the highest surface area show exceptional stability (>100 cycles) and exhibit specific capacities of 710 mAh/g at 0.05 A/g and 150 mAh/g at 1 A/g (Figure 6).

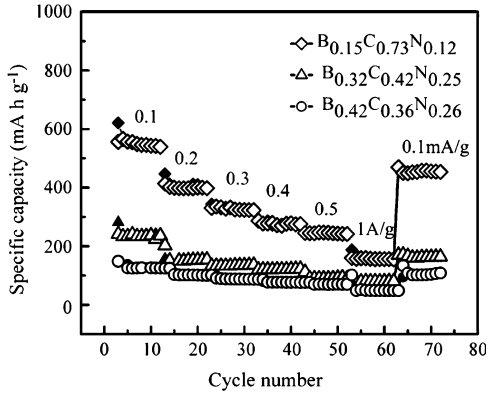

Figure 6. Current rate capabilities of $B_xC_yN_z$ in the range of 0.1−1 A/g. Reprinted with permission from ref 93 (Copyright 2014 WILEY-VCH Verlag GmbH & Co. KGaA, Weinheim).

Layered transition-metal dichalcogenides (TMDs) MX_2 (M = Ti, Nb, Mo, Ta; X = S, Se, Te) act as host lattices to a variety of guest atoms or molecules to yield intercalation compounds wherein the guest species gets inserted between the host layers. Theoretically, the capacity of MoS_2 is only 167 mAh/g if only one mole of Li^+ is intercalated. However, the first discharge capacity of the pristine MoS_2 is slightly above 600 mAh/g with a fast decrease to 200 mAh/g.[94] Restacked MoS_2 electrodes exhibit a reversible specific capacity as high as 710 mAh/g at a current density of 1000 mA/g.[95] Cyclic voltammograms of stacked and restacked MoS_2 are shown in Figure 7(a and b), respectively. Two cathodic peaks at ∼1.0 and 0.4 V in the first cathodic segment are observed due to the decomposition of MoS_2 into Mo nanoparticles. The cyclic performance results are shown in Figure 7(c). For raw MoS_2, the charge capacity obviously decreases with the cycle number from over 800 mAh/g for the first three cycles to 226 mAh/g at the 50th cycle. However, restacked MoS_2 can sustain a high capacity above 750 mAh/g after 50 cycles. Rate capabilities at different current densities are shown in Figure 7(d). MoS_2/C composites prepared by the hydrothermal method employing sodium molybdate, sulfocarbamide, and glucose exhibit excellent reversible capacity (962 mAh/g) and excellent cyclic stability. After 100 cycles, they still retained a capacity of 912 mAh/g.[96] Improvement in the electrochemical properties of MoS_2/a-C composites is due to the synergistic effects of graphene-like MoS_2 and amorphous carbon. The MoS_2/graphene nanocomposite made by the hydrolysis of lithiated MoS_2 ($LiMoS_2$) shows a reversible specific capacity of 1400 mAh/g in the initial cycle and remains at 1351 mAh/g after 200 cycles at 100 mA/g with a cycling performance that is superior to that of bulk MoS_2.[97] In-situ solution-phase reduction method of growing MoS_2 on a graphene composite delivers a high specific capacity of ∼1300 mAh/g.[98] Two-dimensional hybrids with MoS_2 nanocrystals strongly coupled on nitrogen-enriched graphene (MoS_2/NG_g-C_3N_4) are reported to exhibit an outstanding reversible capacity (1450 mAh/g at 0.1 A/g) for 200 cycles and exceptional rate capability (1200 mAh/g at 1A/g, 830 mAh/g at 10 A/g) as an anode in LIBs.[99] MoS_2-coated 3D graphene networks show excellent electrochemical performance with reversible capacities of 877 and 665 mAh/g during the 50th cycle at current densities of 100 and 500 mA/g, respectively.[100]

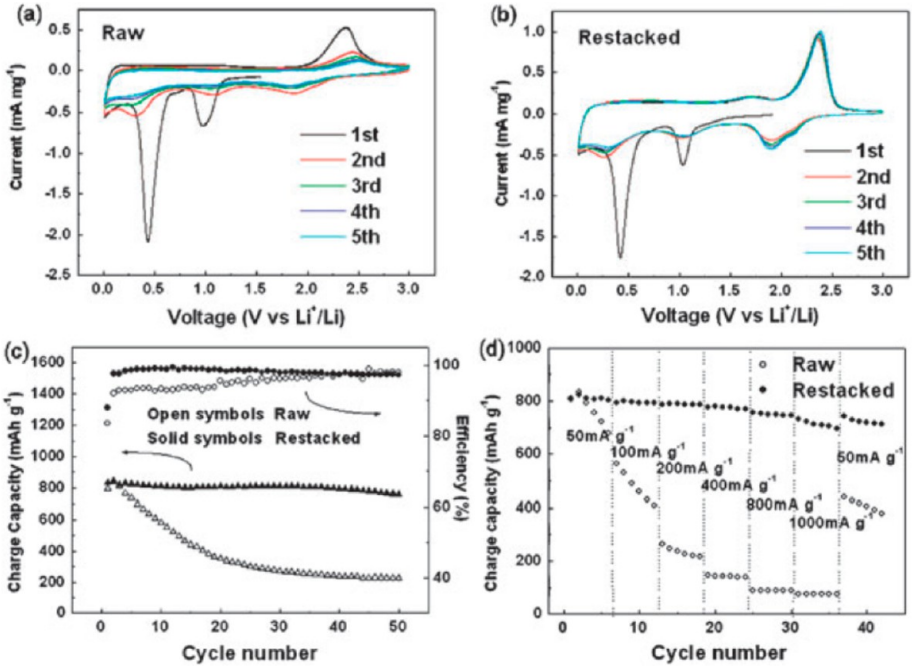

Figure 7. Electrochemical properties of raw and restacked MoS_2 cyclic voltammograms of (a) raw and (b) restacked MoS_2 at a scanning rate of 0.2 mV/s, (c) cycling performances at a current density of 50 mA/g, and (d) rate capabilities at different current densities (discharge current density was kept at 50 mA/g). Reprinted with permission from ref 95 (Copyright 2010 The Royal Society of Chemistry).

DOI: 10.1021/am509096x
ACS Appl. Mater. Interfaces 2015, 7, 7809−7832

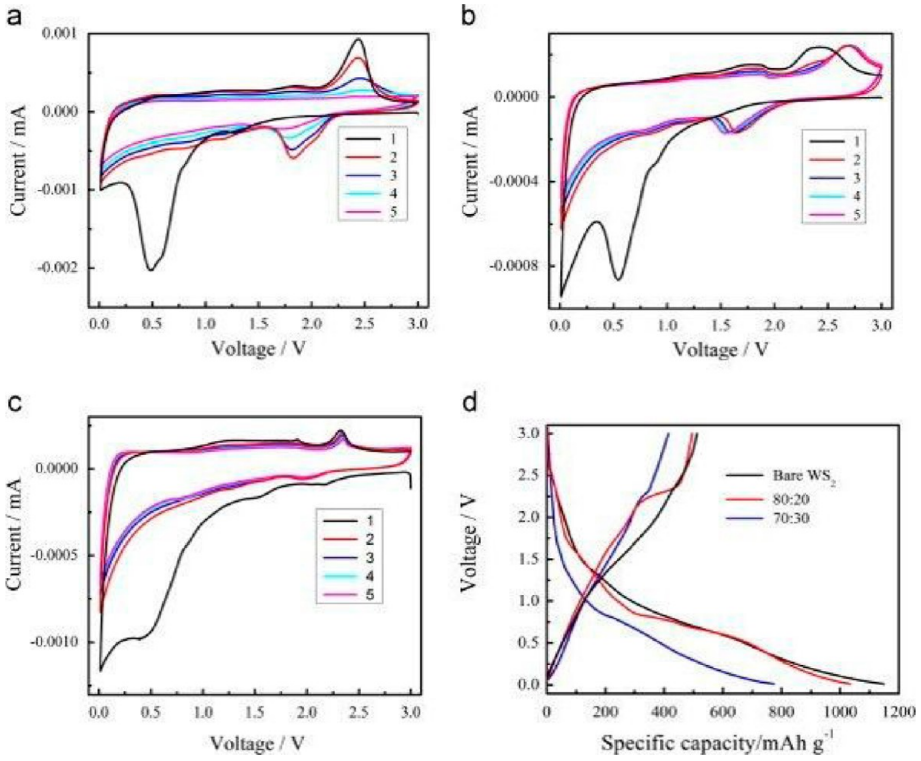

Figure 8. Cyclic voltammograms of (a) bare WS_2, (b) 80:20, and (c) 70:30 electrodes at a scan rate of 0.25 mV/s during the first five cycles. The first charge and discharge curves (d) of bare WS_2, 80:20, and 70:30 at a current density of 100 mA/g. Reprinted with permission from ref 104 (Copyright 2013 Elsevier BV).

WS_2 nanoflakes, prepared using oxalic acid as a reducing reagent in a rheological phase reaction, show improved electrochemical performance.[101] The irreversible capacity in the first cycle is very high (900 mAh/g), but the reversible capacity remained at 680 mAh/g after 20 cycles, which is 86.2% of the initial capacity. Surface-functionalized WS_2 nanosheets show a high first-cycle reversible capacity of 470 mAh/g, which is equivalent to 5.3 Li/WS_2 at a current density of 25 mA/g.[102] The increase in capacity is due to the increased lithium intercalation between the cleaved super acid-treated WS_2 layers. Few-layer WS_2/graphene nanosheet composites prepared by freeze-drying exhibit good cycling stability with a reversible capacity of 647 mAh/g after 80 cycles at a current density of 0.35 A/g.[103] Graphene-like few-layer tungsten sulfide supported on reduced graphene oxide (RGO) by hydrothermal synthesis show a specific capacity of 400−450 mAh/g after 50 cycles at a current density of 100 mA/g.[104] Panels a−c of Figure 8 present cyclic voltammograms of bare WS_2 and WS_2/RGO samples prepared at different compositions for the first 5 cycles. Figure 8(d) shows the first charge and discharge curves of WS_2 and WS_2/RGO composites at a current density of 100 mA/g.

In Table 2, we provide a summary of the properties of Li-batteries based on graphene, MoS_2, and related materials.

Table 2. Performance of Li-Ion Batteries with Graphene, MoS_2, and $B_xC_yN_z$

material	preparation method	specific capacity (mAh/g)	ref
	Graphene		
nitrogen-doped graphene	CVD	684	88
	CVD	1043	89
	thermal	832	90
	hydrothermal	600	91
	hydrothermal	2716	92
borocarbonitrides	CVD	710	93
	MoS_2		
MoS_2 nanosheets	solvothermal	600	94
MoS_2 nanosheets	exfoliation	710	95
MoS_2/C	hydrothermal	962	96
MoS_2/graphene	hydrothermal	1400	105
MoS_2/graphene	solvothermal	1300	98
WS_2 nanosheets	solvothermal	900	101
WS_2 nanosheets	solvothermal	470	102
WS_2/graphene	freeze-drying	647	103
WS_2/graphene	hydrothermal	450	104

5. OXYGEN REDUCTION REACTION (ORR)

A fuel cell is an electrochemical device that generates electricity through the oxidation of a fuel at an anode electrode and reduction of an O_2 at the cathode. The catalyst generally used in ORRs is platinum (Pt). In addition to the high cost, Pt-based catalysts suffer from poor tolerance against carbon monoxide poisoning and fuel crossover. Carbon-based catalysts have shown enhanced catalytic activity equal to that of platinum with low fuel crossover, low cost, and good durability.[106,107] Introduction of nitrogen in the carbon network enhances the ORR activity due to an increase in the electron density of states near the Fermi level. Nitrogen-doped carbon materials, such as carbon nanotubes, carbon nonofibers, and graphene, have been studied.[108] Because the nitrogen in nitrogen-doped graphene is an n-type dopant, it can donate electrons to the neighboring π orbital of conjugated carbon, which in turn provides an electron

DOI: 10.1021/am509096x
ACS Appl. Mater. Interfaces 2015, 7, 7809−7832

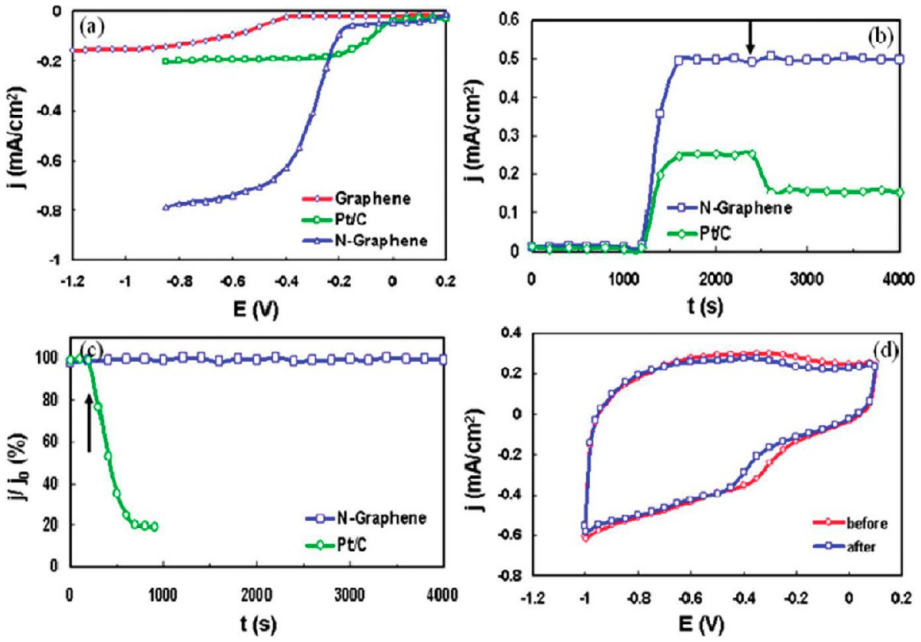

Figure 9. (a) RRDE voltammograms for the ORR in air-saturated 0.1 M KOH at the C-graphene electrode, Pt/C electrode, and N-graphene electrode. (b) Current density (j), time (t) chronoamperometric responses obtained at the Pt/C and N-graphene electrodes at 0.4 V in air saturated 0.1 M KOH. The arrow indicates the addition of 2% (w/w) methanol into the air-saturated electrochemical cell. (c) Current (J) versus time (t) chronoamperometric response of Pt/C and N-graphene electrodes to CO. (d) Cyclic voltammograms of N-graphene electrode in air saturated 0.1 M KOH before and after a continuous potentiodynamic sweep for 200000 cycles at room temperature (25 °C). Scan rate: 0.1 V/s. Reprinted with permission from ref 109 (Copyright 2010 American Chemical Society).

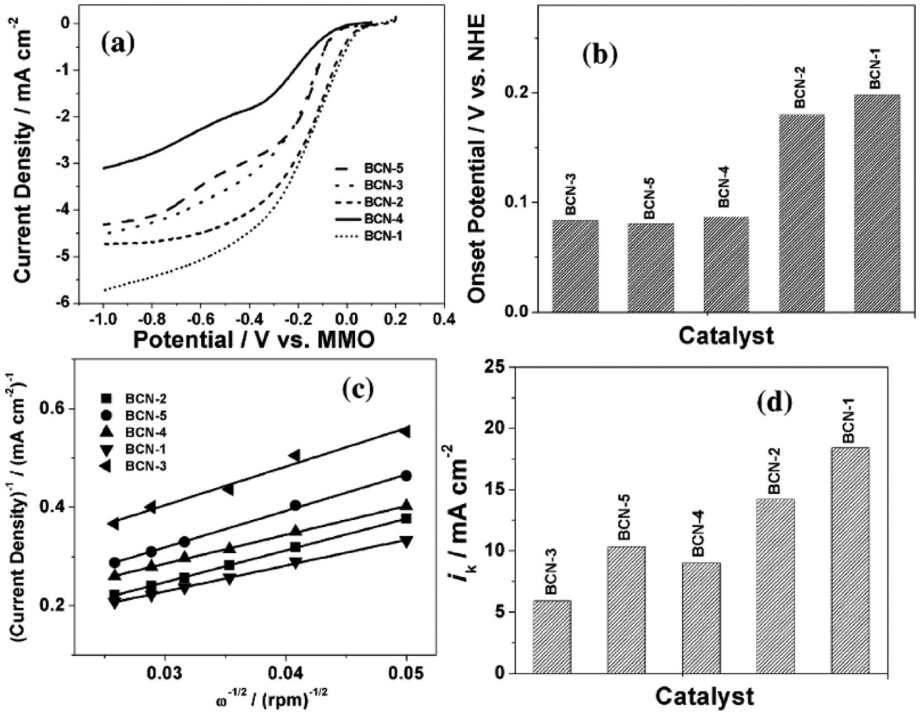

Figure 10. (a) Linear sweep voltammograms obtained with borocarbonitrides (BCNs) recorded at a rotation rate of 1500 rpm and scan rate of 0.005 V/s. (b) Variation of E_{onset} as a function of catalyst. (c) K–L plots obtained at −0.6 V. (d) Variation of i_k obtained using various catalysts in O_2-saturated 0.1m KOH. Reprinted with permission from ref 118 (Copyright 2014 WILEY-VCH Verlag GmbH & Co. KGaA, Weinheim).

to the π^* orbital in the oxygen molecule and thus facilitates splitting.[17]

Dai and co-workers[109] proposed a 4-electron pathway in alkaline solutions for nitrogen-doped graphene, which shows a higher current density and good amperometric response for ORR compared to the commercial platinum–carbon catalyst. Figure 9(a) shows rotating ring-disk electrode (RRDE) voltammograms for the ORR of a N-graphene film for ORR. Electrocatalytic selectivity of the N-graphene electrode against the electro-oxidation of commonly used fuel molecule

DOI: 10.1021/am509096x
ACS Appl. Mater. Interfaces 2015, 7, 7809–7832

Table 3. Oxygen Reduction Reaction Using N-Graphene, BCN, and MoS_2

material	fabrication method	onset potential	current density	electrolyte	ref
N-graphene	RRDE	−0.4 to −0.8 V	−0.8 mA/cm^2	0.1 M KOH	109
	RDE, Hg/HgO	−130 mV		0.1 M KOH	110
	RHE vs Ag/AgCl	0.98 V	−1.1 mA/cm^2	0.1 M KOH	111
	Ag/AgCl	0 to −0.2	−3.5 mA/cm^2	0.1 M KOH	112
	Ag/AgCl	0 to −0.1	−4.2 mA/cm^2	0.1 M KOH	113
	RDE, Ag/AgCl	−0.2 V	−1.2 mA/cm^2	0.1 M KOH	114
B-graphene	RDE, Ag/AgCl	−0.05 V	−5.5 mA/cm^2	0.1 M KOH	115
B,N-graphene	RDE, SCE	−0.16 V,	−6.5 mA/cm^2	0.1 M KOH	116
B,N-graphene	RDE, SCE	0 to −0.2	−5.6 mA/cm^2	0.1 M KOH	117
$B_xC_yN_z$	RDE, Hg/HgO	−0.07 to −0.2	−5.8 mA/cm^2	0.1 M KOH	118
MoS_2/Au	RDE, SCE	−0.10 V		0.1 M KOH	119
MoS_2/RGO	RDE, Ag/AgCl	−0.17	−3 mA/cm^2	0.1 M KOH	67

methanol is shown in Figure 9(b). The N-graphene electrode was insensitive to CO, whereas the Pt/C electrode was rapidly poisoned under the same conditions as shown in Figure 9(c). Potential cycling was carried out to investigate the stability of the N-graphene electrode toward ORR. Figure 9(d) shows the decrease in current observed after 200000 continuous cycles between 1.0 and 0 V in air-saturated 0.1 M KOH electrolyte. Nitrogen plasma-treated graphene exhibits much higher electrocatalytic activity toward oxygen reduction than graphene under alkaline conditions.[110] The ORR overpotential is significantly decreased in N-graphene thereby increasing its electrocatalytic activity with a lower initial electrocatalytic activity than Pt/C but with much higher durability than Pt/C. Nitrogen-doped graphene prepared by the pyrolysis of polyaniline/graphene oxide exhibits excellent ORR catalytic activity comparable to the commercial Pt/C catalyst in alkaline media.[111] Nitrogen-doped graphene with different nitrogen content prepared via high temperature pyrolysis of graphene/polyaniline (PANI) composites exhibits excellent ORR activity in an alkaline electrolyte, including large kinetic-limiting current density and long-term stability as well as the desirable $4e^-$ pathway.[112] Ball milling of graphite powder in the presence of melamine and subsequent heat treatment yields 3.1 at. % nitrogen content at the edge of the graphene matrix.[113] The electrocatalyst exhibits high electrocatalytic activity for ORR due to the synergetic effects of edge N-doping and nanosized graphene platelets. ORR of nitrogen-doped graphene prepared by the pyrolysis of GO-melamine and GO-urea follows a two-electron pathway at low overpotentials but follows the four-electron pathway at higher cathodic potentials.[114] Nitrogen-doped graphene prepared from GO-dicyandiamide follows a four-electron reduction pathway over a wide range of potentials. We have found that heavily N-doped graphene prepared by the microwave method exhibits good ORR activity. It may be recalled that this material is also excellent for supercapacitor applications.[51]

Boron-doped graphene shows good electrocatalytic activity toward oxygen reduction in alkaline conditions similar to the performance of Pt catalysts.[115] Three-dimensional B,N-doped graphene foam performs as an excellent metal-free catalyst for ORR.[116] BCN with tunable B/N codoping levels obtained by thermal annealing GO in the presence of boric acid and ammonia performs as an excellent ORR electrocatalyst.[117] In addition, it shows higher selectivity toward ORR and better methanol tolerance than the commercial Pt/C electrocatalyst. The electron transfer number n of ORR with this BCN/graphene electrocatalyst is close to 4, as determined by the rotating ring disk electrode (RRDE). Composition-dependent ORR activity has been studied in few-layer borocarbonitrides.[118] Figure 10(a) presents linear sweep voltammograms of borocarbonitrides obtained using various catalysts at 1500 rpm. The data reveal that BCN-1 possesses a more positively shifted onset potential with a concomitant increase in current density. Figure 10(b) represents the variation of the onset potential for ORR with the catalysts studied. The onset potential for BCN-1 is ∼0.198 V versus NHE (normal hydrogen electrode) and is more positively shifted. The n value was found to be ∼4 in all compositions (Figure 10(c)). Figure 10(d) shows the variation of i_k obtained using various catalysts in O_2-saturated 0.1 M KOH.

MoS_2 nanoparticles supported on gold nanoparticle films follow a four-electron pathway for the oxygen reduction reaction (ORR) in alkaline media with an onset potential of −0.10 V against the saturated calomel electrode.[119] These films exhibit superior stability and better electrocatalytic performance than commercial Pt/C. MoS_2 particles with different size distributions prepared by simple ultrasonication of bulk MoS_2 showed significantly improved catalytic activity toward the ORR. It is found that a decrease in particle size increases the catalytic activity. Composites of MoS_2 with reduced graphene oxide show good ORR activity.[67] The ORR onset peak potential of MoS_2/RGO is more positive than that of pristine RGO or pristine MoS_2. MoS_2/RGO composites (1:2 and 2:1) demonstrate better ORR activity than either RGO or MoS_2 alone. Such enhanced performance is attributed to a synergistic effect between RGO and MoS_2. The highest reduction potential and current density were obtained with the 1:2 MoS_2/RGO nanocomposites. The 1:2 MoS_2/RGO nanocomposite gives an electron transfer number closer to 4.

Table 3 presents the summary of the results of obtained from the oxygen reduction reaction.

6. HYDROGEN EVOLUTION REACTION (HER)

The necessary condition for any catalyst to act as a hydrogen-evolving catalyst is that the bottom of the conduction band of the catalyst should be more negative than the redox potential of H^+/H_2 (0 V vs NHE at pH 0).[120,121] Efficiency of a HER catalyst is determined by the efficiency of the three steps of HER: (i) photogeneration of electrons and holes, (ii) separation of photogenerated electrons from holes, and (iii) reduction of H^+ to H_2 using the photogenerated electrons.[120] Graphene, with its extraordinarily high electronic conductivity, serves as an ideal electron sink, or rather as an electron transport bridge, thereby enhancing charge separation.

DOI: 10.1021/am509096x
ACS Appl. Mater. Interfaces 2015, 7, 7809−7832

Table 4. Photocatalytic Systems for the Hydrogen Evolution Reaction (HER)

photocatalyst material [cocatalyst]	preparation method	light wavelength [source]	sacrificial agent	activity (mmol/g/h)	ref
		Graphene Sensitized by Semiconductor Nanostructures			
TiO_2/RGO	Sol−gel	UV−Vis [Xe]	Na_2S, Na_2SO_3	0.086	124
TiO_2/RGO	Sol−gel	UV−Vis [Xe]	Na_2S, Na_2SO_3	0.4	125
TiO_2/RGO	self assembly	UV−Vis [Xe]	methanol	0.16	105
P25/RGO	hydrothermal	UV−Vis [Xe]	methanol	0.74	72
GO-coated TiO_2 nanoparticles [Pt]	physical stirring	λ >350 nm	methanol	2	126
TiO_2/RGO [RGO]	microwave-hydrothermal	UV−Vis [Xe]	methanol	0.736	127
N-doped TiO_2	hydrothermal	UV−Vis [Hg/Xe]	methanol	0.716 (UV)/0.112 (Vis)	132
CdS/RGO [Pt]	solvothermal	λ > 420 nm [Xe]	lactic acid	56	128
CdS/RGO [Pt]	two phase solution mixing	λ = 365 nm [Hg]	methanol	5.5	129
CdS/RGO [Pt]	precipitation	λ > 420 nm [Xe]	Na_2S, Na_2SO_3	3.14	130
CdS/RGO	Sol−gel	λ > 420 nm [Xe]	Na_2S, Na_2SO_3	1.66	131
$Zn_xCd_{1-x}S$/RGO	coprecipitation-hydrothermal	λ > 420 nm [Xe]	Na_2S, Na_2SO_3	1.824	123
CdS/Al_2O_3/RGO, CdS/ZnO/RGO	solid state	λ > 420 nm [Xe]	Na_2S, Na_2SO_3	1.750, 3.750	133
CdS/TaON/RGO	hydrothermal	λ > 420 nm [Xe]	Na_2S, Na_2SO_3	3.1650	134
Cu_2O/RGO	in situ	λ > 400 nm [Xe]	methanol	0.2	135
		Dye Sensitized			
EY-RGO [Pt]	in situ photoreduction	$\lambda \geq$ 420 nm [Xe]	TEOA	4.71	140
RB-RGO [Pt]	solution mixing	$\lambda \geq$ 420 nm [Th]	TEOA	1.47	141
EY/RB-RGO [Pt]	in situ photoreduction	$\lambda \geq$ 420 nm [Th]	TEOA	3.67	142
EY-RGO	solution mixing	λ > 320 nm [Xe], λ > 420 nm [Xe]	TEOA	3.35 (UV−Vis), 0.4 (Vis)	189
TPA-RGO	solution mixing	UV−Vis [Xe]	KI	4.6	143
$Ru(dcbpy)_3$-RGO [Pt]	solution mixing	UV−Vis [Xe]	TEOA	1.205	84
$Ru(dcbpy)_3/TiO_2$/RGO [Pt]	colloidal blending	λ > 400 nm [Xe]	EDTA	0.191	139
GO as photocatalyst		UV−Vis [Hg]	MeOH	5.6	144
		MoS_2 Sensitized by Semiconductor Nanostructures			
CdS/MoS_2	impregnation	λ > 420 nm [Xe]	lactic acid	~5.3	177,178
CdSe/MoS_2	assembly	λ > 420 nm [Xe]	Na_2S, Na_2SO_3	0.8	179
SiO_2/MoS_2	thermal decomposition	UV−Vis	Na_2S, Na_2SO_3	0.86	190
TiO_2/MoS_2	thermal decomposition	UV−Vis	lactic acid	0.03	191
TiO_2/MoS_2/graphene	hydrothermal	UV−Vis	ethanol	21	182
		Dye Sensitized			
$Ru(bpy)_3^{2+}$ /Colloidal MoS_2	solvothermal	Vis [Xe]	asorbic acid		180
$Ru(bpy)_3/MoS_xC_y$	solvothermal	Vis [Xe]	triethylamine	19	192
EY/RGO-MoS_2	solvothermal	Vis [Xe]	triethanolamine	2	181
EY/MoS_2	solvothermal	Vis [hal]	triethanolamine	0.05	183
EY/NRGO-MoS_2	solvothermal	Vis [hal], [Xe]	triethanolamine	10.8 (100 W), 42 (400 W)	183
EY/1T- MoS_2	Li intercalation	Vis [hal]	triethanolamine	30 (100 W)	183
EY/$MoSe_2$	solvothermal	Vis [hal]	triethanolamine	0.05 (100 W)	185
EY/1T-$MoSe_2$	Li intercalation	Vis [hal]	triethanolamine	62 ± 5 (100 W)	185
		TMDs as Cocatalysts			
CdS/TiS_2	solution phase	λ > 400 nm [Xe]	benzyl alcohol	1	193
CdS/TaS_2	solution phase	λ > 400 nm [Xe]	benzyl alcohol	2.3	193

Transient photovoltage measurements have provided direct proof of the prolonged mean lifetime of electron−hole pairs to be 10^{-5} s in TiO_2/graphene composites from that of 10^{-5} s in TiO_2.[122] Graphene also acts as a cocatalyst wherein the electrons transferred onto the graphene are directly used for the reduction of protons because the reduction potential of graphene/graphene$^{\bullet-}$ is −0.08 V vs SHE (more negative than H^+/H_2).[123] On the basis of the principles described above, graphene composites with UV and visible light-absorbing semiconductors have been successfully used to improve the photocatalytic efficiency of semiconductors, such as TiO_2,[72,105,124−127] CdS,[128−131] Cu_2O, TaON, and so forth (see Table 4).[121] Figure 11(a) demonstrates the role of graphene in charge separation and as a cocatalyst. The content of graphene in the composites[128] and the method of synthesis play critical roles in determining the efficiency of the catalyst. The importance of the synthetic method is borne out by the fact that different synthetic conditions yield different morphologies and sizes of TiO_2 (or semiconductor) nanoparticles on graphene, thereby causing differences in the activity (see Table 4). Whereas TiO_2/graphene composites can be used only in the UV range, N-doped TiO_2,[132] CdS, and other visible light-absorbing photocatalysts can be used in combination with graphene to produce H_2 using visible light. Construction of heterojunctions of two or more nanostructures also reduces electron hole recombinations due to the built-in electric field at the interface between the two different semiconductors. The addition of graphene to such heterostructures further enhances

DOI: 10.1021/am509096x
ACS Appl. Mater. Interfaces 2015, 7, 7809−7832

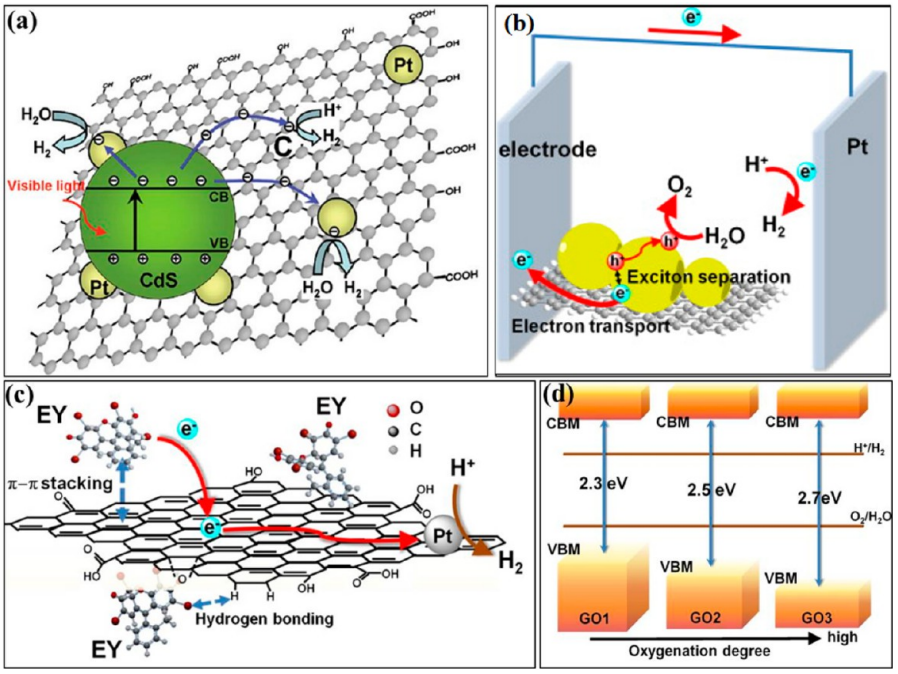

Figure 11. (a) Hydrogen evolution using a graphene/semiconductor system with charge separation and transfer of electrons to graphene in the CdS/RGO system under visible light; proton reduction can happen both on Pt and graphene. Reprinted with permission from ref 128 (Copyright 2011 American Chemical Society). (b) Hydrogen evolution using a photoelectrochemical system with graphene acting as a channel for photogenerated electrons from semiconductor to electrode. Reprinted with permission from ref 120 (Copyright 2013 Elsevier BV). (c) Hydrogen evolution using a dye-sensitized system with electrons that are injected from photoexcited Eosin Y (EY) and subsequently transferred to Pt on which water reduction occurs. Reprinted with permission from ref 120 (Copyright © 2013 Elsevier BV). (d) Hydrogen evolutions using graphene as a photocatalyst with energy level diagrams of RGO with different degrees of reduction in comparison to the potentials for water reduction and oxidation. Reprinted with permission from ref 120 (Copyright © 2013 Elsevier BV).

Table 5. Photo-Electrochemical Hydrogen Evolution Reaction (HER) Systems Using Graphene

photocatalyst	electrolyte	bias	IPCE (%)	ref
TiO_2/RGO	Na_2SO_4	0 (vs Ag/AgCl)	0.0487	194
ZnO/RGO	Na_2SO_4	0.4 (vs Pt)	24 (400 nm)	195
$BiVO_4$/RGO	Na_2SO_4	0.75 (vs Ag/AgCl)	4.2 (400 nm)	136
Fe_2O_3/CNT-RGO	NaOH	1.23 (vs Ag/AgCl)	7 (400 nm)	137
α-Fe_2O_3/RGO	NaOH	0.5 (vs Ag/AgCl)	38 (400 nm)	138

electron transport and thereby increases the yield of H_2.[133,134] Semiconducting Cu_2O[135] and CdS have the perfect conduction band position for HER but cannot be used as stable catalysts for HER because they undergo photocorrosion (oxidization/reduction) by photoinduced e^-/h^+ during photocatalysis, causing degradation of the photocatalytic activity.[121] When used in combination with graphene, photogenerated electrons are transferred to graphene, thereby increasing the stability of the photocatalyst.[121]

Electron accepting and transporting properties of graphene have been exploited not only for photocatalytic water splitting but also for photoelectrochemical H_2 generation (see Table 5). Photocatalysts like $BiVO_4$, WO_3, and Fe_2O_3, which have valence bands (VBs) suitable for water oxidation, are used as anodes in photoelectrochemical cells where water oxidation takes place utilizing the photogenerated holes while H_2 evolution happens at the counter electrode.[12] When graphene is added to such a photocatalyst, it acts as an electron acceptor (see Figure 11(b)), thereby increasing the lifetime of the photogenerated holes. This also provides good electrical contacts with the electrode, enhancing the incident photon-to-current conversion efficiency (IPCE) and reducing the applied external bias.[136−138]

Dye-sensitization is another approach to achieve broad absorption of the solar spectrum used in solar cells. Several wide band gap semiconductors have been used as photocatalysts for HER in the presence of a sensitizer molecule, which upon photoexcitation transfers an electron to the conduction band (CB) of the photocatalyst. The quantum yield (i.e., the photon to energy conversion efficiency of the above process) is limited by the efficiency of electron transfer from the dye to the photocatalyst. The addition of graphene to such a system enhances the photocatalytic yield with graphene acting as the electron transfer channel from the dye to the catalyst.[139] RGOs decorated with Pt nanoparticles have been used for photocatalytic HER using different dye molecules.[140−142] Figure 11(c) gives a schematic picture of dye-sensitized HER with Pt-decorated graphene. Sensitizers like Ru-tris(dicarboxybipyridine) ($Ru(dcbpy)_3$)[84] and 5,10,15,20-tetrakis (4-(hydroxyl)phenyl) porphyrin (TPPH)[39] have been noncovalently linked to RGO followed by Pt impregnation and used for visible light photocatalytic HER. Graphene/dye hybrids like 4-(diphenylamino)benzaldehyde (TPA-CHO)-

DOI: 10.1021/am509096x
ACS Appl. Mater. Interfaces 2015, 7, 7809−7832

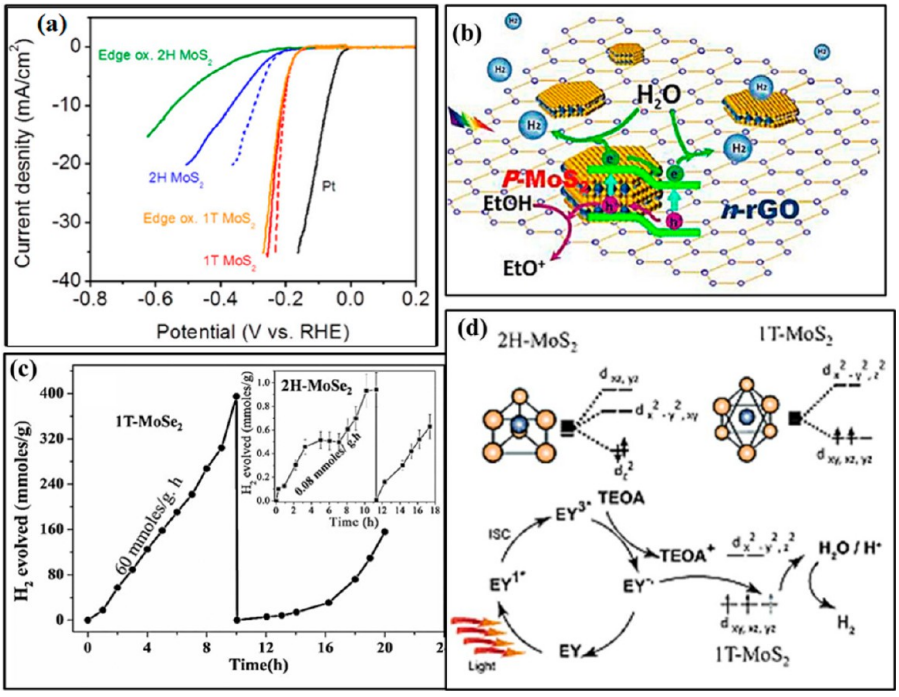

Figure 12. Hydrogen evolution with MoS_2 nanosheets: (a) electrochemical HER with polarization curves of 1T- and 2H-MoS_2 nanosheet electrodes before and after edge oxidation (*iR*-corrected polarization curves from 1T- and 2H-MoS_2 are shown by dashed lines). Reprinted with permission from ref 175 (Copyright 2013 American Chemical Society). (b) p−n junction formed at the interface of MoS_2 and N-doped graphene and its role in charge separation and HER activity. Reprinted with permission from ref 184 (Copyright 2013 American Chemical Society). (c) Schematic representation of electronic structure of 1T- and 2H-MoS_2 and its effect in HER. Reprinted with permission from ref 185 (Copyright 2014 AIP Publishing). (d) Dye-sensitized photocatalytic HER activity of 2H- and 1T-MoS_2. Reprinted with permission from ref 183 (Copyright 2014 WILEY-VCH Verlag GmbH & Co. KGaA, Weinheim).

functionalized graphene prepared by cycloaddition have also been used.[143]

Though graphene is itself a zero band gap material, chemically synthesized graphene oxide (GO) and RGO are semiconductors with the band gap varying with the degree of oxidation. Theoretical and experimental studies have shown that although the VBs of GO and RGO depend directly on the degree of oxidation of the graphene sheet, their CBs are nearly constant with potentials that are more negative than that of proton reduction (see Figure 11(d)).[144−146] Yeh et al.[144] have demonstrated stable H_2 evolution using GO as the photocatalyst with an activity of ∼5.6 mmol/g/h under Hg lamp irradiation with 20 vol % methanol solution as the sacrificial agent even in the absence of any cocatalyst. Under visible light, the activity of GO is found to be much lower than under UV irradiation. Stable O_2 evolution with irradiated GO was also reported using $NaIO_3$ as the sacrificial agent, demonstrating the fact that the VB level of GO is positive enough for O_2 evolution, but the rate of O_2 evolution decreases with the progress of the reaction due to self-reduction of GO, which affects the position of the VB of GO.[147] Dual doped (N, P, or S) graphene showed synergistically enhanced HER activity with robust stability and applicability over a wide range of pH values.[148,149] Deposition of cocatalysts like Ni and NiO can further increase the H_2 evolution by RGO.[150] Nitrogen-doped carbon materials are low-cost electrocatalysts for the oxygen evolution reaction (OER) in alkaline media, and the materials generate a current density of 10 mA/cm^2 at an overpotential of 0.38 V.[151] N,O-dual doped graphene-carbon nanotube (CNT) hydrogel film electrocatalyst fabricated by layer-by-layer assembly of chemically converted graphene and CNTs show enhanced OER activity due to synergy between graphene and CNTs.[152]

Among the layered transition metal dichalcogenides, MoS_2 is a well-known catalyst for the hydrodesulfurization reaction of sulfur-containing aromatic hydrocarbons.[153−155] Co and Ni nanoparticle-decorated few-layer MoS_2 are fine catalysts for hydrodesulfurization of thiophene with ∼98% percent conversion to butane around 375 °C.[156] Hinnemenn et al. first showed that nanoparticles of MoS_2 can be used for electrochemical HER with an overpotential as low as 0.1 V-0.2 V.[157] Theoretical studies have shown that edge sites of MoS_2[158] and vacancy defects[159] are active in HER. Because edges seem to be the catalytically active sites of HER, several studies have been carried out to prepare nanoparticles,[160] nanosheets,[161] and other morphologies[162] with a large density of exposed edges and have been shown to improve both the Tafel slope and the overpotential. An improvement in the electrochemical activity is achieved by increasing the surface area of MoS_2 along with the edge sites.[163−167] The addition of graphene to MoS_2 increases the electronic conductivity of the electrode, thereby improving the overall activity.[61,168] On the basis of the importance of edges in the catalytic activity of MoS_2, several studies have been carried out to understand the nature of edges in MoS_2, and it has been found that edge states in MoS_2 are metallic in nature.[154,169−171]

It has been recently found that monolayers of metallic 1T phases of MoS_2 and WS_2 prepared by chemical exfoliation exhibit superior catalytic activity in electrochemical HER relative to that of the 2H analogue.[172−175] Density functional calculations on the 1T phase of WS_2 has shown that the strained form of 1T state facilitates hydrogen binding and

DOI: 10.1021/am509096x
ACS Appl. Mater. Interfaces 2015, 7, 7809−7832

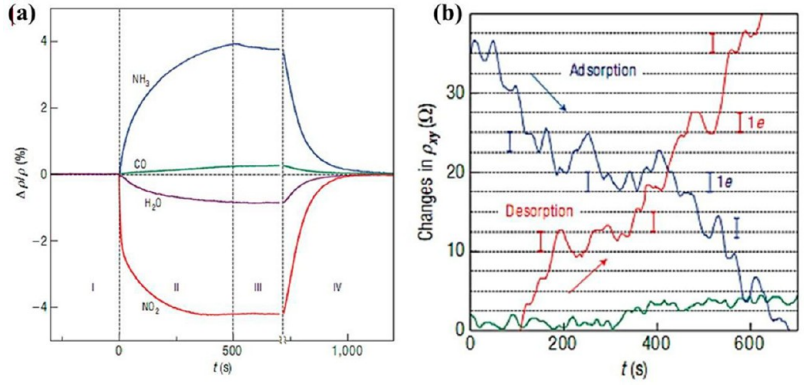

Figure 13. (a) Changes in resistivity, ρ, on exposure of graphene to various gases (1 ppm). Positive (negative) sign indicates electron (hole) doping. Region I, in vacuum; II, exposure to gas; III, evacuation of the experimental setup; and IV, annealing at 150 °C. (b) Change in Hall resistivity, ρ_{xy}, observed near the neutrality point during adsorption and desorption of dilute NO_2. Green curve = reference exposed to pure He. B = 10 T. Grid lines are changes in ρ_{xy} caused by adding one electron charge. Reprinted with permission from ref 202 (Copyright 2007 Nature Publishing Group).

thereby brings the free energy of hydrogen binding close to zero. A hydrogen binding energy of $\Delta G \sim 0$ for a catalyst implies that binding and release of hydrogen by the catalyst are equally easily achieved.[173] Deliberate oxidation of edges of chemically exfoliated MoS_2 has shown that the basal plane of 1T-MoS_2 nanosheets, not the edges, are active in H_2 evolution.[175]

Figure 12(a) compares the electrocatalytic HER activity of 2H- and 1T-MoS_2 with and without edge oxidation. Whereas the catalytic activity of 2H-MoS_2 is mostly dependent on its edges, the basal plane of 1T-MoS_2 determines its catalytic activity. Although the electrochemical HER activity of MoS_2 has been largely studied, photocatalytic and photoelectrochemical HER activity of MoS_2 has not been investigated in detail due to the small band gap of MoS_2 and other layered TMDs.[176] Composites of MoS_2 with good photon-absorbing semiconductors, such as CdS,[177,178] CdSe,[179] TiO_2,[85] and dye-sensitization with $(Ru(bpy)_3)$[180] and eyosin[181] have been employed for HER. As seen earlier, incorporation of a small wt % of graphene with MoS_2 increases the activity because graphene can act as the electron collector, allowing better charge separation.[182] Another effective method of achieving improved charge separation is the creation of a p−n junction by making a composite of p-type MoS_2 with the n-type N-doped graphene. N-doped graphene composites show enhanced photocatalytic activity relative to that of graphene/MoS_2 composites.[183] Similar effects are observed in electrocatalytic HER.[184] Figure 12(b) shows a schematic of the p−n junction formed by MoS_2 with N-doped graphene and its role in charge separation. Photocatalytic HER has been investigated with the chemically exfoliated 1T-form of MoS_2 using eosin Y as the sensitizer. In 1T-MoS_2, Mo lies in an octahedral environment wherein its two electrons lie in the triply degenerate d_{yx}, d_{zx}, d_{zy} orbital. Addition of an extra electron during photocatalysis induces the half-filled configuration d_{xy}, d_{xz}, d_{yz} and increases its stability as shown in Figure 12(d) followed by H_2 evolution. 1T-MoS_2 shows 600 times higher activity than few-layer 2H-MoS_2.[183] 2H- and 1T-forms of $MoSe_2$ have also been studied for HER with an activity of ~62 ± 5 mmol/g/h H_2 (see Figure 12(c)),[185] which is truly impressive. The lower work function of $MoSe_2$ compared to MoS_2 and weaker binding of hydrogen to Se compared to S at the edge sites are considered to be responsible for the greater activity of $MoSe_2$. MoS_2 nanoflowers coated on reduced graphene oxide paper serve as a free-standing, flexible, and durable working electrode for the hydrogen evolution reaction, exhibiting an overpotential lowered to −0.19 V with a Tafel slope of ~95 mV/decade.[186] Whereas most TMDs have been used as photocatalysts, metallic TMDs like TaS_2 and TiS_2 have been used as cocatalyst substitutes for the more costly Pt cocatalysts.[187] Upon addition of TaS_2 or TiS_2 cocatalysts to CdS nanoparticles, the catalytic activity increases from 0.33 mmol/g/h (CdS alone) to 2.3 and 1 mmol/g/h, respectively. MoS_2/CdS nanohybrids prepared by a wet-chemical method possess a large number of edge sites, which act as active sites toward HER under visible light irradiation (>420 nm), and show better activity (16× and 12×, respectively) than pure CdS.[188]

Tables 4 and 5 present a summary of the results of HER carried out photochemically and photoelectrochemically.

7. SENSORS

Graphene has found extensive use in sensing applications.[196−198] The success of graphene as a sensing material stems not only from its high surface area but also from factors such as (a) large conductivity, (b) 2D nature where in it can screen noise better than 1D and 0D structures,[199] and (c) intrinsic ability to interact with molecules via a range of interactions varying from weak van der Waals type to stronger charge transfer type all the way to the strongest covalent bonds.[200] Molecules like water do not induce much change in the localized impurity states in graphene but do change the conductivity.[201] On the other hand, molecules like NO_2, NH_3, alkali elements, and halogens act as dopants and contribute electrons or holes to graphene and change the conductivity. For example, NO_2, an electron-withdrawing molecule, increases the dopant concentration on p-type graphene, thereby increasing its conductivity, whereas NH_3, an electron-donating molecule, decreases the concentration of the dopants in p-type graphene, thereby decreasing its conductivity.[200] High quality single layer graphene was used by Novoselov et al.[202] to prepare gas sensors with a ppb limit of detection (LOD). The device was further optimized using Hall geometry to provide a strong response to change in charge carrier density by operating near the Dirac point.[202] Figure 13(a) shows the response (change in resistance) of the device to various gases, and Figure 13(b) shows the response of the device for adsorption and desorption of NO_2 under the Hall configuration. The device was predicted to show NO_2 detection to the limit of a single NO_2 molecule.

DOI: 10.1021/am509096x
ACS Appl. Mater. Interfaces 2015, 7, 7809−7832

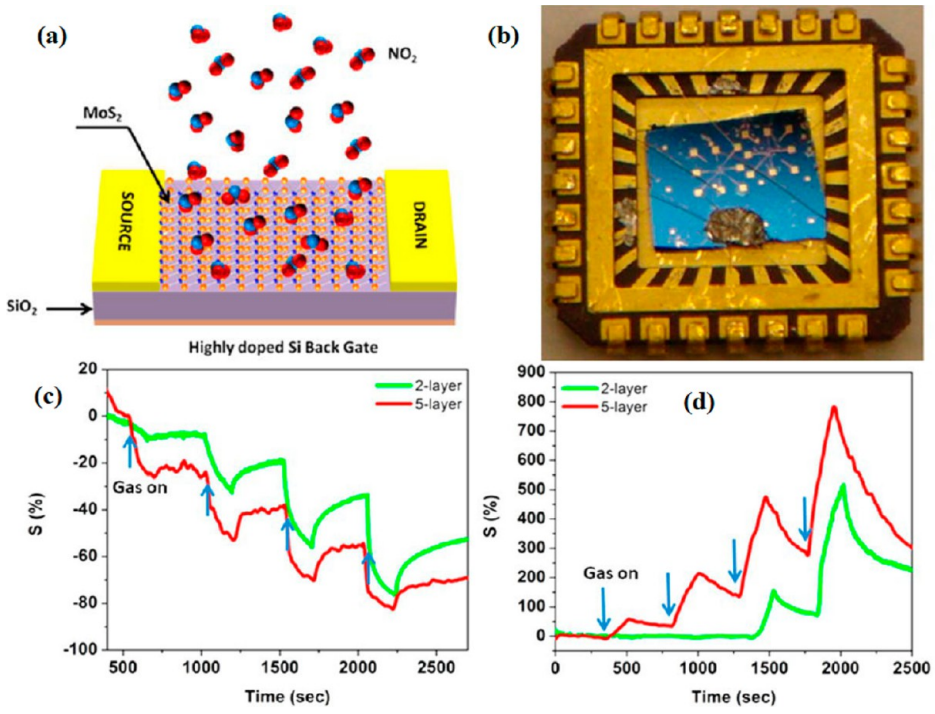

Figure 14. (a) Schematic of the MoS_2 transistor-based NO_2 gas-sensing device. (b) Optical photograph of the MoS_2-sensing device mounted on the chip. Comparative sensing behavior with and without applying back gate voltage (Vg = 15 V) for two-layer MoS_2 for (c) NH_3 and (d) NO_2 (ticks indicate introduction of 100, 200, 500, and 1000 ppm of each gas). Reprinted with permission from ref 223 (Copyright 2013 American Chemical Society).

Pristine single layer graphene has since been used by several groups for sensing gases like NH_3 and CO_2.[203−205]

Transistors with single-layer graphene sense vapors of different small organic molecules, such as THF, CH_3OH, acetonitrile, and chloroform.[206] Furthermore, different vapors induce noise with different frequency characteristics, which can be used as a signal to detect these molecules. Monolayer CVD graphene shows a significant change in the resistance on adsorption of O_2 molecules with an LOD of ∼1.25%.[207] Patterned graphene sensors with vertically aligned graphene sheets prepared via plasma-enhanced CVD have been used to sense NO_2 and NH_3.[208] Pristine CVD graphene is highly sensitive to contaminants like water vapor, which affect the conductance of the sensor. Chen et. al[209] showed that illumination of the device with UV light removes this effect, leading to a sensor with ultrahigh sensitivity of 158 parts per quadrillion (ppq) for NO. The sensor was highly sensitive to NH_3, N_2O, O_2, SO_2, CO_2, and H_2O under flowing N_2 carrier gas with an LOD in the range of 38.8 to 136 ppt.

Single and few-layer graphenes prepared by chemical methods have been used as sensing materials because of the ease of synthesis and fabrication of the devices. Few-layer graphenes prepared by different methods, including thermal exfoliation of graphitic oxide (EG), conversion of nanodiamond (DG), and arc-discharge of graphite in hydrogen (HG), all show significant sensitivity to NO_2 and relative humidity.[210] These sensors also show variation in sensing characteristics with variation of chain length and branching of aliphatic alcohol vapors. The presence of certain defects can enhance the adsorption properties of graphene, thereby affecting the sensing behavior. Nanomesh-like thin films of graphene prepared by CVD of ethanol and CH_4 followed by nanolithographic etching to create edges and defects exhibit 6% and 4.5% response ($\Delta R/R_0$), respectively, whereas no response was observed from unpatterned graphene. RGO-based sensors have the advantage of high electrical conductivity added to their chemically active defect sites, which allow for better gas adsorption. They have been used as highly sensitive sensors for relative humidity[211] and corrosive gases like NO_2 and Cl_2 at low concentrations.[15] However, signal recovery of the RGO-based sensors are generally low because of strong interactions of the gas molecules with defect sites and active functional groups on RGO. Further chemical modifications of RGO, such as sulfonation and ethelyne diamine modification, increase the sensitivity of the device by 4−16 times that of pristine RGO.[212] Few-layer graphene has been effectively used as an electrochemical sensor for DNA bases (guanine, adenine, thymine, and cytosine), oxidase/dehydrogenase-related molecules (hydrogen peroxide (H_2O_2)/β-nicotinamide adenine dinucleotide (NADH)), neurotransmitters (dopamine (DA)), other biological molecules (ascorbic acid (AA), uric acid (UA), and acetaminophen (APAP)), and so forth.[213,214] Well-aligned GO scrolls on hydrophobic substrates, such as the aged gold substrate, polydimethylsiloxane (PDMS) film, poly(L-lactic acid) (PLLA) film, and octadecyltrimethoxysilane (OTS)-modified silicon dioxide, have been used to detect NO_2 at concentrations as low as 0.4 ppm.[215] Solution-processed RGO electrodes with a micropatterned RGO channel with high transparency show good sensitivity in detecting proteins in the physiological buffer (fibronectin) as low as 0.5 nM.[216] Field-effect transistor sensors using micropatterned protein-functionalized RGO films are shown to detect various metal ions (Hg^{2+} and Cd^{2+}) in real-time with high sensitivity.[217] FETs based on RGO patterns are able to detect hormonal catecholamine molecules and their dynamic secretion in living cells.[218] Reduced graphene oxide-modified glassy carbon electrodes

DOI: 10.1021/am509096x
ACS Appl. Mater. Interfaces 2015, 7, 7809−7832

Table 6. Sensing Properties of Graphene and MoS_2

sensor material	target gas	sensitivity and limit of detection		ref
		Graphene		
mechanically exfoliated graphene	NO_2	$\Delta R > 2.5\Omega$ for one electron	single molecule detection	202
mechanically exfoliated graphene	CO_2	$\Delta G/G = 0.17\%$ per ppm		203
mechanically exfoliated graphene	NH_3	charge transfer $f \sim 0.07$ electrons per NH_3		205
mechanically exfoliated graphene	CH_3OH, C_2H_5OH, THF, CH_3CN	frequency vs resistivity pattern variation of each vapor molecule		206
single-layer mechanically exfoliated graphene	O_2	1.25 vol % of gas		207
CVD grown G	NO_2, O_2, SO_2, NO	$\Delta R = 0.2-0.5\%$ ppm^{-1}	158 ppq–103 ppt	209
nanomesh-like CVD-graphene	NO_2	$\Delta R/R_0 = 4.5-6\%$ ppm^{-1}	15 ppb	228
RGO (printable sensor)	NO_2, Cl_2		500 ppb–100 ppm	15
sulfonated/ethelynediamine-modified RGO	NO_2	$\Delta G/G = 0.443$ ppm^{-1}	3.6 ppm	212
		MoS_2		
mechanically exfoliated 1L-MoS_2	selective detection of electron donors like triethylamine, selectivity better than CNT	10 ppb		221
mechanically exfoliated 1–4L-MoS_2	NO		0.3–0.8 ppm	222
mechanically exfoliated 2L- and 5L-MoS_2	NO_2, NH_3, RH	1.37% ppm^{-1}		223

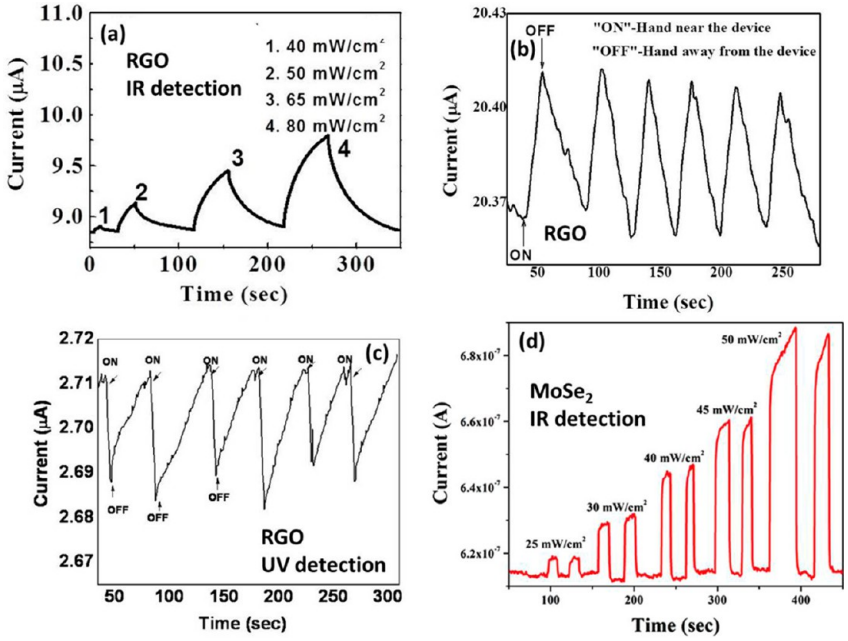

Figure 15. (a) Photocurrent as a function of time with different IR intensities (λ =1550 nm) at 2 V for RGO. (b) Photoresponse of the RGO to a human hand detector at 2 V. Reprinted with permission from ref 233 (Copyright 2011 WILEY-VCH Verlag GmbH & Co. KGaA, Weinheim). (c) Photoresponse of RGO detector to UV light (λ = 360 nm, intensity of 0.3 mW/cm^2) at 2 V. Reprinted with permission from ref 234 (Copyright 2011 AIP Publishing LLC). (d) Photoresponse of few-layer $MoSe_2$-based device with different IR intensities (λ = 1550 nm) at 0.1 V. Reprinted with permission from ref 237 (Copyright 2013 American Chemical Society).

are able detect methicillin-resistant *Staphylococcus aureus* (MRSA) DNA by electrochemical impedance spectroscopy.[218]

Layered MoS_2 has been utilized for sensing a variety of gases. Although natural MoS_2 is an n-type material, chemically prepared MoS_2 behaves as a p-type semiconductor.[219,220] Mechanically exfoliated MoS_2 deposited on a SiO_2/Si substrate behaves as a week n-type material. This can, therefore, show a highly selective response to electron donors like triethylamine but no response to electron acceptors with a selectivity that is much higher than carbon nanotube-based sensors.[221] FET devices with 1–4 layers of mechanically exfoliated MoS_2 have been used as NO sensors[222] with moderate sensitivity and a limit of detection varying from 0.3 to 0.8 ppm depending on the number of layers. Mechanically exfoliated MoS_2 transistors (see Figure 14(a and b)) with varying numbers of layers have been used to detect both electron acceptors like NO_2 and electron donors like NH_3 along with humidity levels under different conditions.[223] NO_2 increases the resistance of the device whereas NH_3 decreases the resistance based on the charge transfer mechanism as shown in Figure 14(c and d). The detection limit could be increased further to 2 ppb using Pt-decorated MoS_2 as the channel. Devices made of electrochemically reduced MoS_2 thin films show good conductivity and fast electron transfer and can be used for selective detection of dopamine and glucose.[224] Single-layer MoS_2 has been used to detect DNA and other biomolecules by making use of

DOI: 10.1021/am509096x
ACS Appl. Mater. Interfaces 2015, 7, 7809–7832

photoluminescence spectra.[225] Single-layer nanosheets of MoS_2, TiS_2, and TaS_2 were used as novel sensing platforms for sensitive and selective detection of DNA based on their high fluorescence-quenching ability and different affinities toward single- and double-stranded DNA.[226] FET sensors based on bilayer (2L), trilayer (3L), and quadrilayer (4L) MoS_2 films exhibit high sensitivity to NO with a detection limit of 0.8 ppm with the single-layer (1L) MoS_2 device showing a rapid but unstable response.[227]

In Table 6, we present a summary of the gas sensing properties of graphene and MoS_2 sheets.

In graphene, optical absorption occurs over a wide wavelength range and has strong interband transitions.[229,230] FET-based ultrafast photodetectors have been prepared using single layer graphene.[231,232] Chemically synthesized reduced graphene oxide, a cheaper and more tunable alternative to mechanically exfoliated single layer graphene, has also been used to prepare scalable and solution processable IR detectors with good photoresponse and significant I_{ON}/I_{OFF} ratios as demonstrated in Figure 15(a). The current responsivity, R_λ, and external quantum efficiency, EQE, were found to be 4 mA/W and 0.3%, respectively.[233] These detectors show strong response to weak IR signals like the human hand (see Figure 15(b)). Detectors, similarly prepared from nanoribbons of graphene (GNR), show even better detection properties with R_λ and EQE of 1 A/W and 80%, respectively, at an IR wavelength of 1550 nm. RGO has also been successfully used for detection of UV radiation (see Figure 15(c)) with R_λ and EQE of 0.12 A/W and 40%, respectively, for UV light with a wavelength of 360 nm and an intensity of 0.3 mW/cm^2.[234]

MoS_2 and other layered TMDs are small band gap semiconductors with properties suitable for photodetector and photovoltaic applications. Single and double-layer MoS_2 has been used as a detector of green light whereas three-layered MoS_2 detects red light.[235] Solution-processable chemically exfoliated MoS_2 was reported to show near an IR absorbance of ~7.8 times greater than reduced graphene oxide.[236] Solution-processable photoresistor devices made from few-layer $MoSe_2$ have been reported to show good IR detection properties (see Figure 15(d)).[237] Phototransistors prepared using single-layer MoS_2 have shown a fast response with a switching duration of 50 ms and good photosensitivity. The responsivity of such devices could be tailored by the gate voltage, making them even better than graphene-based devices.[238] Being a direct band gap semiconductor, single-layer MoS_2 phototransistors with improved contacts and positioning techniques show ~10^6 times better responsivity than graphene.[239] Even phototransistors prepared with few-layer MoS_2 show good detectivity (up to ~10^{10} cm Hz$^{1/2}$/W) and a photoresponsivity of 0.57 A/W due to high optical absorption.[240]

8. CONCLUSIONS

Here, we have presented the unique properties of graphene, transition metal dichalcogenides, and borocarbonitrides that enable many potential applications. Thus, graphene and borocarbonitrides, with large surface areas, can be useful in gas storage with CO_2 sequestration being a possibility. Chemical storage of hydrogen in graphene up to 5 wt % can be useful for various purposes. That these 2D materials exhibit excellent performance in supercapacitors and in the oxygen reduction reaction of fuel cells is truly remarkable. Both of these applications require high electrical conductivity and a large surface area, both of which are provided by these 2D materials. Thus, heavily nitrogenated graphene shows good performance in both supercapacitors and ORRs. Use of these 2D materials in lithium batteries seems attractive and their applications in sensors can indeed be exploited. In particular, radiation sensing (both IR and UV) by graphene is noteworthy. Field effect transistors based on graphene[241] and MoS_2[242] have been fabricated with high mobility and large on–off ratios. The manner in which the study of 2D materials, particularly those of MoS_2 and related materials, has drastically expanded in the last 2 to 3 years promises exciting results in the near future. That 1T-MoS_2 and $MoSe_2$ nanosheets are probably some of the best materials for generating H_2 from water is worth noting. We expect novel discoveries based on valley properties and trions of single-layer MoS_2.[243,244]

AUTHOR INFORMATION

Corresponding Author

*E-mail: cnrrao@jncasr.ac.in. Phone: +91-80-23653075/22082761. Fax: +91-80-22082760.

Notes

The authors declare no competing financial interest.

REFERENCES

(1) Geim, A. K.; Novoselov, K. S. The Rise of Graphene. *Nat. Mater.* **2007**, *6*, 183–191.
(2) Rao, C. N. R.; Maitra, U.; Matte, H. S. S. R. *Synthesis, Characterization, and Selected Properties of Graphene*; Wiley-VCH Verlag GmbH: Weinheim, Germany, 2012.
(3) Huang, X.; Qi, X.; Boey, F.; Zhang, H. Graphene-Based Composites. *Chem. Soc. Rev.* **2012**, *41*, 666–686.
(4) Huang, X.; Yin, Z.; Wu, S.; Qi, X.; He, Q.; Zhang, Q.; Yan, Q.; Boey, F.; Zhang, H. Graphene-Based Materials: Synthesis, Characterization, Properties, and Applications. *Small* **2011**, *7*, 1876–1902.
(5) Chhowalla, M.; Shin, H. S.; Eda, G.; Li, L.-J.; Loh, K. P.; Zhang, H. The Chemistry of Two-Dimensional Layered Transition Metal Dichalcogenide Nanosheets. *Nat. Chem.* **2013**, *5*, 263–275.
(6) Rao, C. N. R.; Maitra, U.; Waghmare, U. V. Extraordinary Attributes of 2-Dimensional MoS_2 Nanosheets. *Chem. Phys. Lett.* **2014**, *609*, 172–183.
(7) Tan, C.; Zhang, H. Two-Dimensional Transition Metal Dichalcogenide Nanosheet-Based Composites. *Chem. Soc. Rev.* **2015**, DOI: 10.1039/C4CS00182F.
(8) Huang, X.; Tan, C.; Yin, Z.; Zhang, H. 25th Anniversary Article: Hybrid Nanostructures Based on Two-Dimensional Nanomaterials. *Adv. Mater.* **2014**, *26*, 2185–2204.
(9) Huang, X.; Zeng, Z.; Zhang, H. Metal Dichalcogenide Nanosheets: Preparation, Properties and Applications. *Chem. Soc. Rev.* **2013**, *42*, 1934–1946.
(10) Editorial: Graphene is not Alone. *Nat. Nanotechnol.* **2012**, *7*, 683–683.
(11) Wang, Q. H.; Kalantar-Zadeh, K.; Kis, A.; Coleman, J. N.; Strano, M. S. Electronics and Optoelectronics of Two-Dimensional Transition Metal Dichalcogenides. *Nat. Nanotechnol.* **2012**, *7*, 699–712.
(12) Maitra, U.; Lingampalli, S. R.; Rao, C. N. R. Artificial Photosynthesis and the Splitting of Water to Generate Hydrogen. *Curr. Sci.* **2014**, *106*, 518–527.
(13) Kumar, N.; Moses, K.; Pramoda, K.; Shirodkar, S. N.; Mishra, A. K.; Waghmare, U. V.; Sundaresan, A.; Rao, C. N. R. Borocarbonitrides, $B_xC_yN_z$. *J. Mater. Chem. A* **2013**, *1*, 5806–5821.
(14) Peigney, A.; Laurent, C.; Flahaut, E.; Bacsa, R. R.; Rousset, A. Specific Surface Area of Carbon Nanotubes and Bundles of Carbon Nanotubes. *Carbon* **2001**, *39*, 507–514.
(15) Dua, V.; Surwade, S. P.; Ammu, S.; Agnihotra, S. R.; Jain, S.; Roberts, K. E.; Park, S.; Ruoff, R. S.; Manohar, S. K. All-Organic Vapor

DOI: 10.1021/am509096x
ACS Appl. Mater. Interfaces 2015, 7, 7809–7832

Sensor Using Inkjet-Printed Reduced Graphene Oxide. *Angew. Chem., Int. Ed.* **2010**, *49*, 2154−2157.
(16) Ghosh, A.; Subrahmanyam, K. S.; Krishna, K. S.; Datta, S.; Govindaraj, A.; Pati, S. K.; Rao, C. N. R. Uptake of H_2 and CO_2 by Graphene. *J. Phys. Chem. C* **2008**, *112*, 15704−15707.
(17) Patchkovskii, S.; Tse, J. S.; Yurchenko, S. N.; Zhechkov, L.; Heine, T.; Seifert, G. Graphene Nanostructures as Tunable Storage Media for Molecular Hydrogen. *Proc. Natl. Acad. Sci. U.S.A.* **2005**, *102*, 10439−10444.
(18) Srinivas, G.; Zhu, Y.; Piner, R.; Skipper, N.; Ellerby, M.; Ruoff, R. Synthesis of Graphene-Like Nanosheets and their Hydrogen Adsorption Capacity. *Carbon* **2010**, *48*, 630−635.
(19) Jin, Z.; Lu, W.; O'Neill, K. J.; Parilla, P. A.; Simpson, L. J.; Kittrell, C.; Tour, J. M. Nano-Engineered Spacing in Graphene Sheets for Hydrogen Storage. *Chem. Mater.* **2011**, *23*, 923−925.
(20) Kumar, R.; Jayaramulu, K.; Maji, T. K.; Rao, C. N. R. Hybrid Nanocomposites of ZIF-8 with Graphene Oxide Exhibiting Tunable Morphology, Significant CO_2 Uptake and other Novel Properties. *Chem. Commun.* **2013**, *49*, 4947−4949.
(21) Mpourmpakis, G.; Tylianakis, E.; Froudakis, G. E. Carbon Nanoscrolls: A Promising Material for Hydrogen Storage. *Nano Lett.* **2007**, *7*, 1893−1897.
(22) Li, J.; Furuta, T.; Goto, H.; Ohashi, T.; Fujiwara, Y.; Yip, S. Theoretical Evaluation of Hydrogen Storage Capacity in Pure Carbon Nanostructures. *J. Chem. Phys.* **2003**, *119*, 2376−2385.
(23) Elias, D. C.; Nair, R. R.; Mohiuddin, T. M. G.; Morozov, S. V.; Blake, P.; Halsall, M. P.; Ferrari, A. C.; Boukhvalov, D. W.; Katsnelson, M. I.; Geim, A. K.; Novoselov, K. S. Control of Graphene's Properties by Reversible Hydrogenation: Evidence for Graphane. *Science* **2009**, *323*, 610−613.
(24) Jaiswal, M.; Lim, C. H. Y. X.; Bao, Q.; Toh, C. T.; Loh, K. P.; Òzyilmaz, B. Controlled Hydrogenation of Graphene Sheets and Nanoribbons. *ACS Nano* **2011**, *5*, 888−896.
(25) Xie, L.; Jiao, L.; Dai, H. Selective Etching of Graphene Edges by Hydrogen Plasma. *J. Am. Chem. Soc.* **2010**, *132*, 14751−14753.
(26) Jones, J. D.; Hoffmann, W. D.; Jesseph, A. V.; Morris, C. J.; Verbeck, G. F.; Perez, J. M. On the Mechanism for Plasma Hydrogenation of Graphene. *Appl. Phys. Lett.* **2010**, *97*, 233103−233104.
(27) Zheng, L.; Li, Z.; Bourdo, S.; Watanabe, F.; Ryerson, C. C.; Biris, A. S. Catalytic Hydrogenation of Graphene Films. *Chem. Commun.* **2011**, *47*, 1213−1215.
(28) Subrahmanyam, K. S.; Kumar, P.; Maitra, U.; Govindaraj, A.; Hembram, K. P. S. S.; Waghmare, U. V.; Rao, C. N. R. Chemical Storage of Hydrogen in Few-Layer Graphene. *Proc. Natl. Acad. Sci. U.S.A.* **2011**, *108*, 2674−2677.
(29) Raidongia, K.; Nag, A.; Hembram, K. P.; Waghmare, U. V.; Datta, R.; Rao, C. N.R BCN: A Graphene Analogue with Remarkable Adsorptive Properties. *Chemistry* **2010**, *4*, 149−57.
(30) Kumar, N.; Subrahmanyam, K. S.; Chaturbedy, P.; Raidongia, K.; Govindaraj, A.; Hembram, K. P. S. S.; Mishra, A. K.; Waghmare, U. V.; Rao, C. N. R. Remarkable Uptake of CO_2 and CH_4 by Graphene-Like Borocarbonitrides, $B_xC_yN_z$. *ChemSusChem* **2011**, *4*, 1662−1670.
(31) Kotz, R.; Carlen, M. Principles and Applications of Electrochemical Capacitors. *Electrochim. Acta* **2000**, *45*, 2483−2498.
(32) Wang, G.; Zhang, L.; Zhang, J. A Review of Electrode Materials for Electrochemical Supercapacitors. *Chem. Soc. Rev.* **2012**, *41*, 797−828.
(33) Cao, X.; Yin, Z.; Zhang, H. Three-Dimensional Graphene Materials: Preparation, Structures and Application in Supercapacitors. *Energy Environ. Sci.* **2014**, *7*, 1850−1865.
(34) Stoller, M. D.; Park, S.; Zhu, Y.; An, J.; Ruoff, R. S. Graphene-Based Ultracapacitors. *Nano Lett.* **2008**, *8*, 3498−3502.
(35) Wang, Y.; Shi, Z.; Huang, Y.; Ma, Y.; Wang, C.; Chen, M.; Chen, Y. Supercapacitor Devices Based on Graphene Materials. *J. Phys. Chem. C* **2009**, *113*, 13103−13107.
(36) Zhu, Y.; Murali, S.; Stoller, M. D.; Velamakanni, A.; Piner, R. D.; Ruoff, R. S. Microwave Assisted Exfoliation and Reduction of Graphite Oxide for Ultracapacitors. *Carbon* **2010**, *48*, 2118−2122.
(37) Zhu, Y.; Murali, S.; Stoller, M. D.; Ganesh, K. J.; Cai, W.; Ferreira, P. J.; Pirkle, A.; Wallace, R. M.; Cychosz, K. A.; Thommes, M.; Su, D.; Stach, E. A.; Ruoff, R. S. Carbon-Based Supercapacitors Produced by Activation of Graphene. *Science* **2011**, *332*, 1537−1541.
(38) Liu, C.; Yu, Z.; Neff, D.; Zhamu, A.; Jang, B. Z. Graphene-Based Supercapacitor with an Ultrahigh Energy Density. *Nano Lett.* **2010**, *10*, 4863−4868.
(39) Wang, X.; Zhang, Y.; Zhi, C.; Wang, X.; Tang, D.; Xu, Y.; Weng, Q.; Jiang, X.; Mitome, M.; Golberg, D.; Bando, Y. Three-Dimensional Strutted Graphene Grown by Substrate-Free Sugar Blowing for High-Power-Density Supercapacitors. *Nat. Commun.* **2013**, *4*, 2905.
(40) Sun, Y.; Wu, Q.; Shi, G. Supercapacitors Based on Self-Assembled Graphene Organogel. *Phys. Chem. Chem. Phys.* **2011**, *13*, 17249−17254.
(41) Zhang, J.; Tian, T.; Chen, Y.; Niu, Y.; Tang, J.; Qin, L.-C. Synthesis of Graphene from Dry Ice in Flames and its Application in Supercapacitors. *Chem. Phys. Lett.* **2014**, *591*, 78−81.
(42) Cao, X.; Shi, Y.; Shi, W.; Lu, G.; Huang, X.; Yan, Q.; Zhang, Q.; Zhang, H. Preparation of Novel 3D Graphene Networks for Supercapacitor Applications. *Small* **2011**, *7*, 3163−3168.
(43) Maiti, U. N.; Lim, J.; Lee, K. E.; Lee, W. J.; Kim, S. O. Three-Dimensional Shape Engineered, Interfacial Gelation of Reduced Graphene Oxide for High Rate, Large Capacity Supercapacitors. *Adv. Mater.* **2014**, *26*, 615−619.
(44) Lee, Y. J.; Kim, G.-P.; Bang, Y.; Yi, J.; Seo, J. G.; Song, I. K. Activated Carbon Aerogel Containing Graphene as Electrode Material for Supercapacitor. *Mater. Res. Bull.* **2014**, *50*, 240−245.
(45) Peng, Y.-Y.; Liu, Y.-M.; Chang, J.-K.; Wu, C.-H.; Ger, M.-D.; Pu, N.-W.; Chang, C.-L. A Facile Approach to Produce Holey Graphene and Its Application in Supercapacitors. *Carbon* **2014**, *81*, 347−356.
(46) Jana, M.; Khanra, P.; Murmu, N. C.; Samanta, P.; Lee, J. H.; Kuila, T. Covalent Surface Modification of Chemically Derived Graphene and Its Application as Supercapacitor Electrode Material. *Phys. Chem. Chem. Phys.* **2014**, *16*, 7618−7626.
(47) Liu, W.-w.; Yan, X.-b.; Lang, J.-w.; Pu, J.-b.; Xue, Q.-j. Supercapacitors Based on Graphene Nanosheets Using Different Non-Aqueous Electrolytes. *New J. Chem.* **2013**, *37*, 2186−2195.
(48) Wang, H.; Maiyalagan, T.; Wang, X. Review on Recent Progress in Nitrogen-Doped Graphene: Synthesis, Characterization, and Its Potential Applications. *ACS Catal.* **2012**, *2*, 781−794.
(49) Lei, Z.; Lu, L.; Zhao, X. S. The Electrocapacitive Properties of Graphene Oxide Reduced by Urea. *Energy Environ. Sci.* **2012**, *5*, 6391−6399.
(50) Gopalakrishnan, K.; Moses, K.; Govindaraj, A.; Rao, C. N. R. Supercapacitors Based on Nitrogen-Doped Reduced Graphene Oxide And Borocarbonitrides. *Solid State Commun.* **2013**, *175−176*, 43−50.
(51) Gopalakrishnan, K.; Govindaraj, A.; Rao, C. N. R. Extraordinary Supercapacitor Performance of Heavily Nitrogenated Graphene Oxide Obtained by Microwave Synthesis. *J. Mater. Chem. A* **2013**, *1*, 7563−7565.
(52) Sun, L.; Wang, L.; Tian, C.; Tan, T.; Xie, Y.; Shi, K.; Li, M.; Fu, H. Nitrogen-Doped Graphene with High Nitrogen Level via a One-Step Hydrothermal Reaction of Graphene Oxide with Urea for Superior Capacitive Energy Storage. *RSC Adv.* **2012**, *2*, 4498−4506.
(53) Zuo, Z.; Jiang, Z.; Manthiram, A. Porous B-doped Graphene Inspired by Fried-Ice for Supercapacitors and Metal-Free Catalysts. *J. Mater. Chem. A* **2013**, *1*, 13476−13483.
(54) Niu, L.; Li, Z.; Hong, W.; Sun, J.; Wang, Z.; Ma, L.; Wang, J.; Yang, S. Pyrolytic Synthesis of Boron-Doped Graphene and Its Application as Electrode Material For Supercapacitors. *Electrochim. Acta* **2013**, *108*, 666−673.
(55) Soon, J. M.; Loh, K. P. Electrochemical Double-Layer Capacitance of MoS_2 Nanowall Films. *Electrochem. Solid-State Lett.* **2007**, *10*, A250−A254.
(56) Cao, L.; Yang, S.; Gao, W.; Liu, Z.; Gong, Y.; Ma, L.; Shi, G.; Lei, S.; Zhang, Y.; Zhang, S.; Vajtai, R.; Ajayan, P. M. Direct Laser-Patterned Micro-Supercapacitors from Paintable MoS_2 Films. *Small* **2013**, *9*, 2905−2910.

DOI: 10.1021/am509096x
ACS Appl. Mater. Interfaces 2015, 7, 7809−7832

(57) Krishnamoorthy, K.; Veerasubramani, G. K.; Radhakrishnan, S.; Kim, S. J. Supercapacitive Properties of Hydrothermally Synthesized Sphere Like MoS_2 Nanostructures. *Mater. Res. Bull.* **2014**, *50*, 499−502.
(58) Zhou, X.; Xu, B.; Lin, Z.; Shu, D.; Ma, L. Hydrothermal Synthesis of Flower-Like MoS_2 Nanospheres for Electrochemical Supercapacitors. *J. Nanosci. Nanotechnol.* **2014**, *14*, 7250−7254.
(59) Yang, Y.; Fei, H.; Ruan, G.; Xiang, C.; Tour, J. M. Edge-Oriented MoS_2 Nanoporous Films as Flexible Electrodes for Hydrogen Evolution Reactions and Supercapacitor Devices. *Adv. Mater.* **2014**, *26*, 8163−8168.
(60) Ramadoss, A.; Kim, T.; Kim, G.-S.; Kim, S. J. Enhanced Activity of A Hydrothermally Synthesized Mesoporous MoS_2 Nanostructure for High Performance Supercapacitor Applications. *New J. Chem.* **2014**, *38*, 2379−2385.
(61) Li, Y.; Wang, H.; Xie, L.; Liang, Y.; Hong, G.; Dai, H. MoS_2 Nanoparticles Grown on Graphene: An Advanced Catalyst for the Hydrogen Evolution Reaction. *J. Am. Chem. Soc.* **2011**, *133*, 7296−7299.
(62) Sun, G.; Liu, J.; Zhang, X.; Wang, X.; Li, H.; Yu, Y.; Huang, W.; Zhang, H.; Chen, P. Fabrication of Ultralong Hybrid Microfibers from Nanosheets of Reduced Graphene Oxide and Transition-Metal Dichalcogenides and their Application as Supercapacitors. *Angew. Chem., Int. Ed.* **2014**, *53*, 12576−12580.
(63) Hu, B.; Qin, X.; Asiri, A. M.; Alamry, K. A.; Al-Youbi, A. O.; Sun, X. Synthesis of Porous Tubular C/MoS_2 Nanocomposites and Their Application as A Novel Electrode Material for Supercapacitors with Excellent Cycling Stability. *Electrochim. Acta* **2013**, *100*, 24−28.
(64) da Silveira Firmiano, E. G.; Rabelo, A. C.; Dalmaschio, C. J.; Pinheiro, A. N.; Pereira, E. C.; Schreiner, W. H.; Leite, E. R. Supercapacitor Electrodes Obtained by Directly Bonding 2D MoS_2 on Reduced Graphene Oxide. *Adv. Energy Mater.* **2014**, *4*, 1301380.
(65) Patil, S.; Harle, A.; Sathaye, S.; Patil, K. Development of A Novel Method to Grow Mono-/Few-Layered MoS_2 Films and MoS_2-Graphene Hybrid Films for Supercapacitor Applications. *CrystEngComm* **2014**, *16*, 10845−10855.
(66) Huang, K.-J.; Wang, L.; Liu, Y.-J.; Liu, Y.-M.; Wang, H.-B.; Gan, T.; Wang, L.-L. Layered MoS_2@Graphene Composites for Supercapacitor Applications with Enhanced Capacitive Performance. *Int. J. Hydrogen Energy* **2013**, *38*, 14027−14034.
(67) Gopalakrishnan, K.; Pramoda, K.; Urmimala, M.; Mahima, U.; Shah, M. A.; Rao, C. N. R. Performance of MoS_2-Reduced Graphene Oxide Nanocomposites in Supercapacitors and in Oxygen Reduction Reaction. *Nanomater. Energy* **2014**, DOI: 10.1680/nme.14.00024.
(68) Gopalakrishnan, K.; Sultan, S.; Govindaraj, A.; Rao, C. N. R. Supercapacitors Based on Composites of PANI with Nanosheets of Nitrogen-Doped RGO, $BC_{1.5}N$, MoS_2 and WS_2. *Nano Energy* **2015**, *12*, 52−58.
(69) Tang, H.; Wang, J.; Yin, H.; Zhao, H.; Wang, D.; Tang, Z. Growth of Polypyrrole Ultrathin Films on MoS_2 Monolayers as High-Performance Supercapacitor Electrodes. *Adv. Mater.* **2015**, *27*, 1117−1123.
(70) Vivekchand, S. R. C.; Rout, C.; Subrahmanyam, K. S.; Govindaraj, A.; Rao, C. N. R. Graphene-Based Electrochemical Supercapacitors. *J. Chem. Sci.* **2008**, *120*, 9−13.
(71) Wang, M.; Oh, J.; Ghosh, T.; Hong, S.; Nam, G.; Hwang, T.; Nam, J.-D. An Interleaved Porous Laminate Composed of Reduced Graphene Oxide Sheets and Carbon Black Spacers by In Situ Electrophoretic Deposition. *RSC Adv.* **2014**, *4*, 3284−3292.
(72) Fan, W.; Lai, Q.; Zhang, Q.; Wang, Y. Nanocomposites of TiO_2 and Reduced Graphene Oxide as Efficient Photocatalysts for Hydrogen Evolution. *J. Phys. Chem. C* **2011**, *115*, 10694−10701.
(73) Jung, N.; Kwon, S.; Lee, D.; Yoon, D.-M.; Park, Y. M.; Benayad, A.; Choi, J.-Y.; Park, J. S. Synthesis of Chemically Bonded Graphene/Carbon Nanotube Composites and their Application in Large Volumetric Capacitance Supercapacitors. *Adv. Mater.* **2013**, *25*, 6854−6858.
(74) Yang, S.-Y.; Chang, K.-H.; Tien, H.-W.; Lee, Y.-F.; Li, S.-M.; Wang, Y.-S.; Wang, J.-Y.; Ma, C.-C. M.; Hu, C.-C. Design and Tailoring of A Hierarchical Graphene-Carbon Nanotube Architecture for Supercapacitors. *J. Mater. Chem.* **2011**, *21*, 2374−2380.
(75) Cheng, Q.; Tang, J.; Ma, J.; Zhang, H.; Shinya, N.; Qin, L.-C. Graphene and Carbon Nanotube Composite Electrodes for Supercapacitors with Ultra-High Energy Density. *Phys. Chem. Chem. Phys.* **2011**, *13*, 17615−17624.
(76) Guo, H.-L.; Su, P.; Kang, X.; Ning, S.-K. Synthesis and Characterization of Nitrogen-Doped Graphene Hydrogels by Hydrothermal Route with Urea as Reducing-Doping Agents. *J. Mater. Chem. A* **2013**, *1*, 2248−2255.
(77) Hassan, F. M.; Chabot, V.; Li, J.; Kim, B. K.; Ricardez-Sandoval, L.; Yu, A. Pyrrolic-Structure Enriched Nitrogen Doped Graphene for Highly Efficient Next Generation Supercapacitors. *J. Mater. Chem. A* **2013**, *1*, 2904−2912.
(78) Rao, C. N. R.; Gopalakrishnan, K.; Govindaraj, A. Synthesis, Properties and Applications of Graphene Doped with Boron, Nitrogen and Other Elements. *Nano Today* **2014**, *9*, 324−343.
(79) Jeong, H. M.; Lee, J. W.; Shin, W. H.; Choi, Y. J.; Shin, H. J.; Kang, J. K.; Choi, J. W. Nitrogen-Doped Graphene for High-Performance Ultracapacitors and the Importance of Nitrogen-Doped Sites at Basal Planes. *Nano Lett.* **2011**, *11*, 2472−2477.
(80) Nolan, H.; Mendoza-Sanchez, B.; Ashok Kumar, N.; McEvoy, N.; O'Brien, S.; Nicolosi, V.; Duesberg, G. S. Nitrogen-Doped Reduced Graphene Oxide Electrodes for Electrochemical Supercapacitors. *Phys. Chem. Chem. Phys.* **2014**, *16*, 2280−2284.
(81) Wen, Z.; Wang, X.; Mao, S.; Bo, Z.; Kim, H.; Cui, S.; Lu, G.; Feng, X.; Chen, J. Crumpled Nitrogen-Doped Graphene Nanosheets with Ultrahigh Pore Volume for High-Performance Supercapacitor. *Adv. Mater.* **2012**, *24*, 5610−5616.
(82) Qiu, Y.; Zhang, X.; Yang, S. High Performance Supercapacitors Based on Highly Conductive Nitrogen-Doped Graphene Sheets. *Phys. Chem. Chem. Phys.* **2011**, *13*, 12554−12558.
(83) Chang, Y.; Han, G.; Fu, D.; Liu, F.; Li, M.; Li, Y. Larger-Scale Fabrication of N-Doped Graphene-Fiber Mats Used in High-Performance Energy Storage. *J. Power Sources* **2014**, *252*, 113−121.
(84) Zhu, M.; Dong, Y.; Xiao, B.; Du, Y.; Yang, P.; Wang, X. Enhanced Photocatalytic Hydrogen Evolution Performance Based on Ru-Trisdicarboxybipyridine-Reduced Graphene Oxide Hybrid. *J. Mater. Chem.* **2012**, *22*, 23773−23779.
(85) Zhou, W.; Yin, Z.; Du, Y.; Huang, X.; Zeng, Z.; Fan, Z.; Liu, H.; Wang, J.; Zhang, H. Synthesis of Few-Layer MoS_2 Nanosheet-Coated TiO_2 Nanobelt Heterostructures for Enhanced Photocatalytic Activities. *Small* **2013**, *9*, 140−147.
(86) Zhu, J.; Yang, D.; Yin, Z.; Yan, Q.; Zhang, H. Graphene and Graphene-Based Materials for Energy Storage Applications. *Small* **2014**, *10*, 3480−3498.
(87) Reddy, A. L. M.; Srivastava, A.; Gowda, S. R.; Gullapalli, H.; Dubey, M.; Ajayan, P. M. Synthesis Of Nitrogen-Doped Graphene Films For Lithium Battery Application. *ACS Nano* **2010**, *4*, 6337−6342.
(88) Wang, H.; Zhang, C.; Liu, Z.; Wang, L.; Han, P.; Xu, H.; Zhang, K.; Dong, S.; Yao, J.; Cui, G. Nitrogen-Doped Graphene Nanosheets with Excellent Lithium Storage Properties. *J. Mater. Chem.* **2011**, *21*, 5430−5434.
(89) Wu, Z.-S.; Ren, W.; Xu, L.; Li, F.; Cheng, H.-M. Doped Graphene Sheets As Anode Materials with Superhigh Rate and Large Capacity for Lithium Ion Batteries. *ACS Nano* **2011**, *5*, 5463−5471.
(90) Tian, L.-L.; Wei, X.-Y.; Zhuang, Q.-C.; Jiang, C.-H.; Wu, C.; Ma, G.-Y.; Zhao, X.; Zong, Z.-M.; Sun, S.-G. Bottom-Up Synthesis of Nitrogen-Doped Graphene Sheets for Ultrafast Lithium Storage. *Nanoscale* **2014**, *6*, 6075−6083.
(91) Du, M.; Sun, J.; Chang, J.; Yang, F.; Shi, L.; Gao, L. Synthesis of Nitrogen-Doped Reduced Graphene Oxide Directly from Nitrogen-Doped Graphene Oxide as a High-Performance Lithium Ion Battery Anode. *RSC Adv.* **2014**, *4*, 42412−42417.
(92) Jiang, Z.; Jiang, Z.-J.; Tian, X.; Luo, L. Nitrogen-doped Graphene Hollow Microspheres as an Efficient Electrode Material for Lithium Ion Batteries. *Electrochim. Acta* **2014**, *146*, 455−463.

DOI: 10.1021/am509096x
ACS Appl. Mater. Interfaces 2015, 7, 7809−7832

(93) Sen, S.; Moses, K.; Bhattacharyya, A. J.; Rao, C. N. R. Excellent Performance of Few-Layer Borocarbonitrides as Anode Materials in Lithium-Ion Batteries. *Chem.—Asian J.* **2014**, *9*, 100−103.
(94) Hwang, H.; Kim, H.; Cho, J. MoS_2 Nanoplates Consisting of Disordered Graphene-like Layers for High Rate Lithium Battery Anode Materials. *Nano Lett.* **2011**, *11*, 4826−4830.
(95) Du, G.; Guo, Z.; Wang, S.; Zeng, R.; Chen, Z.; Liu, H. Superior Stability and High Capacity of Restacked Molybdenum Disulfide as Anode Material for Lithium Ion Batteries. *Chem. Commun.* **2010**, *46*, 1106−1108.
(96) Chang, K.; Chen, W.; Ma, L.; Li, H.; Li, H.; Huang, F.; Xu, Z.; Zhang, Q.; Lee, J.-Y. Graphene-Like MoS_2/Amorphous Carbon Composites with High Capacity and Excellent Stability as Anode Materials for Lithium Ion Batteries. *J. Mater. Chem.* **2011**, *21*, 6251−6257.
(97) Liu, Y.; Zhao, Y.; Jiao, L.; Chen, J. A Graphene-Like MoS_2/Graphene Nanocomposite as a Highperformance Anode For Lithium Ion Batteries. *J. Mater. Chem. A* **2014**, *2*, 13109−13115.
(98) Chang, K.; Chen, W. In Situ Synthesis of MoS_2/Graphene Nanosheet Composites with Extraordinarily High Electrochemical Performance for Lithium Ion Batteries. *Chem.Commun.* **2011**, *47*, 4252−4254.
(99) Tang, Y.; Wu, D.; Mai, Y.; Pan, H.; Cao, J.; Yang, C.; Zhang, F.; Feng, X. A Two-Dimensional Hybrid with Molybdenum Disulfide Nanocrystals Strongly Coupled on Nitrogen-Enriched Graphene Via Mild Temperature Pyrolysis for High Performance Lithium Storage. *Nanoscale* **2014**, *6*, 14679−14685.
(100) Cao, X.; Shi, Y.; Shi, W.; Rui, X.; Yan, Q.; Kong, J.; Zhang, H. Preparation of MoS_2-Coated Three-Dimensional Graphene Networks for High-Performance Anode Material in Lithium-Ion Batteries. *Small* **2013**, *9*, 3433−3438.
(101) Feng, C.; Huang, L.; Guo, Z.; Liu, H. Synthesis of Tungsten Disulfide (WS_2) Nanoflakes for Lithium Ion Battery Application. *Electrochem. Commun.* **2007**, *9*, 119−122.
(102) Bhandavat, R.; David, L.; Singh, G. Synthesis of Surface-Functionalized WS_2 Nanosheets and Performance as Li-Ion Battery Anodes. *J. Phys.Chem. Lett.* **2012**, *3*, 1523−1530.
(103) Xu, X.; Rout, C. S.; Yang, J.; Cao, R.; Oh, P.; Shin, H. S.; Cho, J. Freeze-Dried WS_2 Composites with Low Content of Graphene as High-Rate Lithium Storage Materials. *J. Mater. Chem. A* **2013**, *1*, 14548−14554.
(104) Shiva, K.; Ramakrishna Matte, H. S. S.; Rajendra, H. B.; Bhattacharyya, A. J.; Rao, C. N. R. Employing Synergistic Interactions Between Few-Layer WS_2 and Reduced Graphene Oxide to Improve Lithium Storage, Cyclability and Rate Capability of Li-Ion Batteries. *Nano Energy* **2013**, *2*, 787−793.
(105) Li, N.; Liu, G.; Zhen, C.; Li, F.; Zhang, L.; Cheng, H.-M. Battery Performance and Photocatalytic Activity of Mesoporous Anatase TiO_2 Nanospheres/Graphene Composites by Template-Free Self-Assembly. *Adv. Funct. Mater.* **2011**, *21*, 1717−1722.
(106) Kou, R.; Shao, Y.; Wang, D.; Engelhard, M. H.; Kwak, J. H.; Wang, J.; Viswanathan, V. V.; Wang, C.; Lin, Y.; Wang, Y.; Aksay, I. A.; Liu, J. Enhanced Activity and Stability of Pt Catalysts on Functionalized Graphene Sheets for Electrocatalytic Oxygen Reduction. *Electrochem. Commun.* **2009**, *11*, 954−957.
(107) Daems, N.; Sheng, X.; Vankelecom, I. F. J.; Pescarmona, P. P. Metal-Free Doped Carbon Materials as Electrocatalysts for The Oxygen Reduction Reaction. *J. Mater. Chem. A* **2014**, *2*, 4085−4110.
(108) Kundu, S.; Nagaiah, T. C.; Xia, W.; Wang, Y.; Dommele, S. V.; Bitter, J. H.; Santa, M.; Grundmeier, G.; Bron, M.; Schuhmann, W.; Muhler, M. Electrocatalytic Activity and Stability of Nitrogen-Containing Carbon Nanotubes in the Oxygen Reduction Reaction. *J. Phys. Chem. C* **2009**, *113*, 14302−14310.
(109) Qu, L.; Liu, Y.; Baek, J.-B.; Dai, L. Nitrogen-Doped Graphene as Efficient Metal-Free Electrocatalyst for Oxygen Reduction in Fuel Cells. *ACS Nano* **2010**, *4*, 1321−1326.
(110) Shao, Y.; Zhang, S.; Engelhard, M. H.; Li, G.; Shao, G.; Wang, Y.; Liu, J.; Aksay, I. A.; Lin, Y. Nitrogen-Doped Graphene and Its Electrochemical Applications. *J. Mater. Chem.* **2010**, *20*, 7491−7496.
(111) Mo, Z.; Zheng, R.; Peng, H.; Liang, H.; Liao, S. Nitrogen-Doped Graphene Prepared by A Transfer Doping Approach for the Oxygen Reduction Reaction Application. *J. Power Sources* **2014**, *245*, 801−807.
(112) Liu, M.; Song, Y.; He, S.; Tjiu, W. W.; Pan, J.; Xia, Y.-Y.; Liu, T. Nitrogen-Doped Graphene Nanoribbons as Efficient Metal-Free Electrocatalysts for Oxygen Reduction. *ACS Appl. Mater. Interfaces* **2014**, *6*, 4214−4222.
(113) Fu, X.; Jin, J.; Liu, Y.; Wei, Z.; Pan, F.; Zhang, J. Efficient Oxygen Reduction Electrocatalyst Based on Edge-Nitrogen-Rich Graphene Nanoplatelets: Toward a Large-Scale Synthesis. *ACS Appl. Mater. Interfaces* **2014**, *6*, 3930−3936.
(114) Vikkisk, M.; Kruusenberg, I.; Joost, U.; Shulga, E.; Kink, I.; Tammeveski, K. Electrocatalytic Oxygen Reduction on Nitrogen-Doped Graphene in Alkaline Media. *Appl. Catal., B* **2014**, *147*, 369−376.
(115) Sheng, Z.-H.; Gao, H.-L.; Bao, W.-J.; Wang, F.-B.; Xia, X.-H. Synthesis of Boron Doped Graphene for Oxygen Reduction Reaction in Fuel Cells. *J. Mater. Chem.* **2012**, *22*, 390−395.
(116) Xue, Y.; Yu, D.; Dai, L.; Wang, R.; Li, D.; Roy, A.; Lu, F.; Chen, H.; Liu, Y.; Qu, J. Three-Dimensional B,N-Doped Graphene Foam as a Metal-Free Catalyst for Oxygen Reduction Reaction. *Phys. Chem. Chem. Phys.* **2013**, *15*, 12220−12226.
(117) Wang, S.; Zhang, L.; Xia, Z.; Roy, A.; Chang, D. W.; Baek, J.-B.; Dai, L. BCN Graphene as Efficient Metal-Free Electrocatalyst for the Oxygen Reduction Reaction. *Angew. Chem., Int. Ed.* **2012**, *51*, 4209−4212.
(118) Moses, K.; Kiran, V.; Sampath, S.; Rao, C. N. R. Few-Layer Borocarbonitride Nanosheets: Platinum-Free Catalyst for the Oxygen Reduction Reaction. *Chem.—Asian J.* **2014**, *9*, 838−843.
(119) Wang, T.; Zhuo, J.; Chen, Y.; Du, K.; Papakonstantinou, P.; Zhu, Z.; Shao, Y.; Li, M. Synergistic Catalytic Effect of MoS_2 Nanoparticles Supported on Gold Nanoparticle Films for a Highly Efficient Oxygen Reduction Reaction. *Chem. Catal. Chem.* **2014**, *6*, 1877−1881.
(120) Yeh, T.-F.; Cihlář, J.; Chang, C.-Y.; Cheng, C.; Teng, H. Roles of Graphene Oxide in Photocatalytic Water Splitting. *Mater. Today* **2013**, *16*, 78−84.
(121) Xie, G.; Zhang, K.; Guo, B.; Liu, Q.; Fang, L.; Gong, J. R. Graphene-Based Materials for Hydrogen Generation from Light-Driven Water Splitting. *Adv. Mater.* **2013**, *25*, 3820−3839.
(122) Jiang, B.; Tian, C.; Pan, Q.; Jiang, Z.; Wang, J.-Q.; Yan, W.; Fu, H. Enhanced Photocatalytic Activity and Electron Transfer Mechanisms of Graphene/TiO_2 with Exposed {001} Facets. *J. Phys. Chem. C* **2011**, *115*, 23718−23725.
(123) Zhang, J.; Yu, J.; Jaroniec, M.; Gong, J. R. Noble Metal-Free Reduced Graphene Oxide-ZnxCd1−xS Nanocomposite with Enhanced Solar Photocatalytic H_2-Production Performance. *Nano Lett.* **2012**, *12*, 4584−4589.
(124) Zhang, X.-Y.; Li, H.-P.; Cui, X.-L.; Lin, Y. Graphene/TiO_2 Nanocomposites: Synthesis, Characterization and Application in Hydrogen Evolution from Water Photocatalytic Splitting. *J. Mater. Chem.* **2010**, *20*, 2801−2806.
(125) Shen, J.; Shi, M.; Yan, B.; Ma, H.; Li, N.; Ye, M. Ionic Liquid-Assisted One-Step Hydrothermal Synthesis of TiO_2-Reduced Graphene Oxide Composites. *Nano Res.* **2011**, *4*, 795−806.
(126) Kim, H.-i.; Moon, G.-h.; Monllor-Satoca, D.; Park, Y.; Choi, W. Solar Photoconversion Using Graphene/TiO_2 Composites: Nanographene Shell on TiO_2 Core versus TiO_2 Nanoparticles on Graphene Sheet. *J. Phys. Chem. C* **2012**, *116*, 1535−1543.
(127) Xiang, Q.; Yu, J.; Jaroniec, M. Enhanced Photocatalytic H_2-Production Activity of Graphene-Modified Titania Nanosheets. *Nanoscale* **2011**, *3*, 3670−3678.
(128) Li, Q.; Guo, B.; Yu, J.; Ran, J.; Zhang, B.; Yan, H.; Gong, J. R. Highly Efficient Visible-Light-Driven Photocatalytic Hydrogen Production of CdS-Cluster-Decorated Graphene Nanosheets. *J. Am. Chem. Soc.* **2011**, *133*, 10878−10884.

DOI: 10.1021/am509096x
ACS Appl. Mater. Interfaces 2015, 7, 7809−7832

(129) Gao, P.; Liu, J.; Lee, S.; Zhang, T.; Sun, D. D. High Quality Graphene Oxide-CdS-Pt Nanocomposites for Efficient Photocatalytic Hydrogen Evolution. *J. Mater. Chem.* **2012**, *22*, 2292−2298.
(130) Peng, T.; Li, K.; Zeng, P.; Zhang, Q.; Zhang, X. Enhanced Photocatalytic Hydrogen Production over Graphene Oxide−Cadmium Sulfide Nanocomposite under Visible Light Irradiation. *J. Phys. Chem. C* **2012**, *116*, 22720−22726.
(131) Lv, X.-J.; Fu, W.-F.; Chang, H.-X.; Zhang, H.; Cheng, J.-S.; Zhang, G.-J.; Song, Y.; Hu, C.-Y.; Li, J.-H. Hydrogen Evolution from Water Using Semiconductor Nanoparticle/Graphene Composite Photocatalysts Without Noble Metals. *J. Mater. Chem.* **2012**, *22*, 1539−1546.
(132) Pei, F.; Liu, Y.; Xu, S.; Lü, J.; Wang, C.; Cao, S. Nanocomposite of Graphene Oxide with Nitrogen-Doped TiO_2 Exhibiting Enhanced Photocatalytic Efficiency for Hydrogen Evolution. *Int. J. Hydrogen Energy* **2013**, *38*, 2670−2677.
(133) Khan, Z.; Chetia, T. R.; Vardhaman, A. K.; Barpuzary, D.; Sastri, C. V.; Qureshi, M. Visible Light Assisted Photocatalytic Hydrogen Generation and Organic Dye Degradation by CdS-Metal Oxide Hybrids in Presence of Graphene Oxide. *RSC Adv.* **2012**, *2*, 12122−12128.
(134) Hou, J.; Wang, Z.; Kan, W.; Jiao, S.; Zhu, H.; Kumar, R. V. Efficient Visible-Light-Driven Photocatalytic Hydrogen Production Using CdS@TaON Core-Shell Composites Coupled with Graphene Oxide Nanosheets. *J. Mater. Chem.* **2012**, *22*, 7291−7299.
(135) Tran, P. D.; Batabyal, S. K.; Pramana, S. S.; Barber, J.; Wong, L. H.; Loo, S. C. J. A Cuprous Oxide-Reduced Graphene Oxide (Cu_2O-rGO) Composite Photocatalyst for Hydrogen Generation: Employing rGO as an Electron Acceptor to Enhance the Photocatalytic Activity and Stability of Cu_2O. *Nanoscale* **2012**, *4*, 3875−3878.
(136) Ng, Y. H.; Iwase, A.; Kudo, A.; Amal, R. Reducing Graphene Oxide on a Visible-Light $BiVO_4$ Photocatalyst for an Enhanced Photoelectrochemical Water Splitting. *J. Phys. Chem. Lett.* **2010**, *1*, 2607−2612.
(137) Young Kim, J.; Jang, J.-W.; Hyun Youn, D.; Yul Kim, J.; Sun Kim, E.; Sung Lee, J. Graphene-Carbon Nanotube Composite as an Effective Conducting Scaffold to Enhance the Photoelectrochemical Water Oxidation Activity of a Hematite Film. *RSC Adv.* **2012**, *2*, 9415−9422.
(138) Zhang, K.; Shi, X.; Kim, J. K.; Lee, J. S.; Park, J. H. Inverse Opal Structured -Fe_2O_3 on Graphene Thin Films: Enhanced Photo-Assisted Water Splitting. *Nanoscale* **2013**, *5*, 1939−1944.
(139) Chen, Y.; Mou, Z.; Yin, S.; Huang, H.; Yang, P.; Wang, X.; Du, Y. Graphene Enhanced Photocatalytic Hydrogen Evolution Performance of Dye-Sensitized TiO_2 Under Visible Light Irradiation. *Mater. Lett.* **2013**, *107*, 31−34.
(140) Min, S.; Lu, G. Dye-Sensitized Reduced Graphene Oxide Photocatalysts for Highly Efficient Visible-Light-Driven Water Reduction. *J. Phys. Chem. C* **2011**, *115*, 13938−13945.
(141) Min, S.; Lu, G. Promoted Photoinduced Charge Separation and Directional Electron Transfer Over Dispersible Xanthene Dyes Sensitized Graphene Sheets for Efficient Solar H_2 Evolution. *Int. J. Hyd. Energy* **2013**, *38*, 2106−2116.
(142) Min, S.; Lu, G. Dye-Cosensitized Graphene/Pt Photocatalyst for High Efficient Visible Light Hydrogen Evolution. *Int. J. Hyd. Energy* **2012**, *37*, 10564−10574.
(143) Li, Z.; Chen, Y.; Du, Y.; Wang, X.; Yang, P.; Zheng, J. Triphenylamine-Functionalized Graphene Decorated with Pt Nanoparticles and Its Application in Photocatalytic Hydrogen Production. *Int. J. Hydrogen Energy* **2012**, *37*, 4880−4888.
(144) Yeh, T.-F.; Syu, J.-M.; Cheng, C.; Chang, T.-H.; Teng, H. Graphite Oxide as a Photocatalyst for Hydrogen Production from Water. *Adv. Funct. Mater.* **2010**, *20*, 2255−2262.
(145) Zhan, D.; Ni, Z.; Chen, W.; Sun, L.; Luo, Z.; Lai, L.; Yu, T.; Wee, A. T. S.; Shen, Z. Electronic Structure of Graphite Oxide and Thermally Reduced Graphite Oxide. *Carbon* **2011**, *49*, 1362−1366.
(146) Mkhoyan, K. A.; Contryman, A. W.; Silcox, J.; Stewart, D. A.; Eda, G.; Mattevi, C.; Miller, S.; Chhowalla, M. Atomic and Electronic Structure of Graphene-Oxide. *Nano Lett.* **2009**, *9*, 1058−1063.
(147) Yeh, T.-F.; Chan, F.-F.; Hsieh, C.-T.; Teng, H. Graphite Oxide with Different Oxygenated Levels for Hydrogen and Oxygen Production from Water under Illumination: The Band Positions of Graphite Oxide. *J. Phys. Chem. C* **2011**, *115*, 22587−22597.
(148) Zheng, Y.; Jiao, Y.; Li, L. H.; Xing, T.; Chen, Y.; Jaroniec, M.; Qiao, S. Z. Toward Design of Synergistically Active Carbon-Based Catalysts for Electrocatalytic Hydrogen Evolution. *ACS Nano* **2014**, *8*, 5290−5296.
(149) Ito, Y.; Cong, W.; Fujita, T.; Tang, Z.; Chen, M. High Catalytic Activity of Nitrogen and Sulfur Co-Doped Nanoporous Graphene in the Hydrogen Evolution Reaction. *Angew. Chem., Int. Ed.* **2015**, *54*, 2131−2136.
(150) Agegnehu, A. K.; Pan, C.-J.; Rick, J.; Lee, J.-F.; Su, W.-N.; Hwang, B.-J. Enhanced Hydrogen Generation by Cocatalytic Ni and NiO Nanoparticles Loaded on Graphene Oxide Sheets. *J. Mater. Chem.* **2012**, *22*, 13849−13854.
(151) Zhao, Y.; Nakamura, R.; Kamiya, K.; Nakanishi, S.; Hashimoto, K. Nitrogen-Doped Carbon Nanomaterials as Non-Metal Electrocatalysts for Water Oxidation. *Nat. Commun.* **2013**, *4*, 2390.
(152) Chen, S.; Duan, J.; Jaroniec, M.; Qiao, S.-Z. Nitrogen and Oxygen Dual-Doped Carbon Hydrogel Film as a Substrate-Free Electrode for Highly Efficient Oxygen Evolution Reaction. *Adv. Mater.* **2014**, *26*, 2925−2930.
(153) Prins, R. Catalytic Hydrodenitrogenation. *Adv. Catal.* **2001**, *46*, 399−464.
(154) Lauritsen, J. V.; Nyberg, M.; Nørskov, J. K.; Clausen, B. S.; Topsøe, H.; Lægsgaard, E.; Besenbacher, F. Hydrodesulfurization Reaction Pathways on MoS_2 Nanoclusters Revealed by Scanning Tunneling Microscopy. *J. Catal.* **2004**, *224*, 94−106.
(155) Tsverin, Y.; Popovitz-Biro, R.; Feldman, Y.; Tenne, R.; Komarneni, M. R.; Yu, Z.; Chakradhar, A.; Sand, A.; Burghaus, U. Synthesis and Characterization of WS_2 Nanotube Supported Cobalt Catalyst for Hydrodesulfurization. *Mater. Res. Bull.* **2012**, *47*, 1653−1660.
(156) Rao, B. G.; Matte, H. S. S. R.; Chaturbedy, P.; Rao, C. N. R. Hydrodesulfurization of Thiophene Over Few-Layer MoS_2 Covered with Co and Ni Nanoparticles. *ChemPlusChem.* **2013**, *78*, 419−422.
(157) Hinnemann, B.; Moses, P. G.; Bonde, J.; Jørgensen, K. P.; Nielsen, J. H.; Horch, S.; Chorkendorff, I.; Nørskov, J. K. Biomimetic Hydrogen Evolution: MoS_2 Nanoparticles as Catalyst for Hydrogen Evolution. *J. Am. Chem. Soc.* **2005**, *127*, 5308−5309.
(158) Jaramillo, T. F.; Jørgensen, K. P.; Bonde, J.; Nielsen, J. H.; Horch, S.; Chorkendorff, I. Identification of Active Edge Sites for Electrochemical H_2 Evolution from MoS_2 Nanocatalysts. *Science* **2007**, *317*, 100−102.
(159) Ataca, C.; Ciraci, S. Dissociation of H_2O at the Vacancies of Single-Layer MoS_2. *Phys. Rev. B* **2012**, *85*, 195410.
(160) Wang, D.; Wang, Z.; Wang, C.; Zhou, P.; Wu, Z.; Liu, Z. Distorted MoS_2 Nanostructures: An Efficient Catalyst for the Electrochemical Hydrogen Evolution Reaction. *Electrochem. Commun.* **2013**, *34*, 219−222.
(161) Kong, D.; Wang, H.; Cha, J. J.; Pasta, M.; Koski, K. J.; Yao, J.; Cui, Y. Synthesis of MoS_2 and $MoSe_2$ Films with Vertically Aligned Layers. *Nano Lett.* **2013**, *13*, 1341−1347.
(162) Kibsgaard, J.; Chen, Z.; Reinecke, B. N.; Jaramillo, T. F. Engineering the Surface Structure of MoS_2 to Preferentially Expose Active Edge Sites for Electrocatalysis. *Nat. Mater.* **2012**, *11*, 963−969.
(163) Merki, D.; Hu, X. Recent Developments of Molybdenum and Tungsten Sulfides as Hydrogen Evolution Catalysts. *Energy Environ. Sci.* **2011**, *4*, 3878−3888.
(164) Laursen, A. B.; Kegnaes, S.; Dahl, S.; Chorkendorff, I. Molybdenum Sulfides-Efficient and Viable Materials for Electro - and Photoelectrocatalytic Hydrogen Evolution. *Energy Environ. Sci.* **2012**, *5*, 5577−5591.
(165) Merki, D.; Fierro, S.; Vrubel, H.; Hu, X. Amorphous Molybdenum Sulfide Films as Catalysts for Electrochemical Hydrogen Production in Water. *Chem. Sci.* **2011**, *2*, 1262−1267.

DOI: 10.1021/am509096x
ACS Appl. Mater. Interfaces 2015, 7, 7809−7832

(166) Rao, C. N. R.; Matte, H. S. S. R.; Maitra, U. Graphene Analogues of Inorganic Layered Materials. *Angew. Chem., Int. Ed.* **2013**, *52*, 13162−13185.
(167) Lau, V. W.-h.; Masters, A. F.; Bond, A. M.; Maschmeyer, T. Ionic-Liquid-Mediated Active-Site Control of MoS_2 for the Electrocatalytic Hydrogen Evolution Reaction. *Chem.—Eur. J.* **2012**, *18*, 8230−8239.
(168) Firmiano, E. G. S.; Cordeiro, M. A. L.; Rabelo, A. C.; Dalmaschio, C. J.; Pinheiro, A. N.; Pereira, E. C.; Leite, E. R. Graphene Oxide as a Highly Selective Substrate to Synthesize a Layered MoS_2 Hybrid Electrocatalyst. *Chem. Commun.* **2012**, *48*, 7687−7689.
(169) Lauritsen, J. V.; Nyberg, M.; Vang, R. T.; Bollinger, M. V.; Clausen, B. S.; Topsøe, H.; Jacobsen, K. W.; Lægsgaard, E.; Nørskov, J. K.; Besenbacher, F. Chemistry of One-Dimensional Metallic Edge States in MoS_2 Nanoclusters. *Nanotechnology* **2003**, *14*, 385.
(170) Kibsgaard, J.; Lauritsen, J. V.; Lægsgaard, E.; Clausen, B. S.; Topsøe, H.; Besenbacher, F. Cluster−Support Interactions and Morphology of MoS_2 Nanoclusters in a Graphite-Supported Hydrotreating Model Catalyst. *J. Am. Chem. Soc.* **2006**, *128*, 13950−13958.
(171) Hansen, L. P.; Ramasse, Q. M.; Kisielowski, C.; Brorson, M.; Johnson, E.; Topsøe, H.; Helveg, S. Atomic-Scale Edge Structures on Industrial-Style MoS_2 Nanocatalysts. *Angew. Chem., Int. Ed.* **2011**, *50*, 10153−10156.
(172) Lukowski, M. A.; Daniel, A. S.; Meng, F.; Forticaux, A.; Li, L.; Jin, S. Enhanced Hydrogen Evolution Catalysis from Chemically Exfoliated Metallic MoS_2 Nanosheets. *J. Am. Chem. Soc.* **2013**, *135*, 10274−10277.
(173) Voiry, D.; Yamaguchi, H.; Li, J.; Silva, R.; Alves, D. C. B.; Fujita, T.; Chen, M.; Asefa, T.; Shenoy, V. B.; Eda, G.; Chhowalla, M. Enhanced Catalytic Activity in Strained Chemically Exfoliated WS_2 Nanosheets for Hydrogen Evolution. *Nat. Mater.* **2013**, *12*, 850−855.
(174) Lukowski, M. A.; Daniel, A. S.; English, C. R.; Meng, F.; Forticaux, A.; Hamers, R. J.; Jin, S. Highly Active Hydrogen Evolution Catalysis from Metallic WS_2 Nanosheets. *Energy Environ. Sci.* **2014**, *7*, 2608−2613.
(175) Voiry, D.; Salehi, M.; Silva, R.; Fujita, T.; Chen, M.; Asefa, T.; Shenoy, V. B.; Eda, G.; Chhowalla, M. Conducting MoS_2 Nanosheets as Catalysts for Hydrogen Evolution Reaction. *Nano Lett.* **2013**, *13*, 6222−6227.
(176) Debbichi, L.; Eriksson, O.; Lebègue, S. Electronic Structure of Two-Dimensional Transition Metal Dichalcogenide Bilayers from *Ab Initio* Theory. *Phys. Rev. B* **2014**, *89*, 205311.
(177) Zong, X.; Yan, H.; Wu, G.; Ma, G.; Wen, F.; Wang, L.; Li, C. Enhancement of Photocatalytic H_2 Evolution on CdS by Loading MoS_2 as Cocatalyst under Visible Light Irradiation. *J. Am. Chem. Soc.* **2008**, *130*, 7176−7177.
(178) Zong, X.; Wu, G.; Yan, H.; Ma, G.; Shi, J.; Wen, F.; Wang, L.; Li, C. Photocatalytic H_2 Evolution on MoS_2/CdS Catalysts under Visible Light Irradiation. *J. Phys. Chem. C* **2010**, *114*, 1963−1968.
(179) Frame, F. A.; Osterloh, F. E. CdSe-MoS_2: A Quantum Size-Confined Photocatalyst for Hydrogen Evolution from Water under Visible Light. *J. Phys. Chem. C* **2010**, *114*, 10628−10633.
(180) Zong, X.; Na, Y.; Wen, F.; Ma, G.; Yang, J.; Wang, D.; Ma, Y.; Wang, M.; Sun, L.; Li, C. Visible Light Driven H_2 Production in Molecular Systems Employing Colloidal MoS_2 Nanoparticles as Catalyst. *Chem. Commun.* **2009**, 4536−4538.
(181) Min, S.; Lu, G. Sites for High Efficient Photocatalytic Hydrogen Evolution on a Limited-Layered MoS_2 Cocatalyst Confined on Graphene Sheets——The Role of Graphene. *J. Phys. Chem. C* **2012**, *116*, 25415−25424.
(182) Xiang, Q.; Yu, J.; Jaroniec, M. Synergetic Effect of MoS_2 and Graphene as Cocatalysts for Enhanced Photocatalytic H_2 Production Activity of TiO_2 Nanoparticles. *J. Am. Chem. Soc.* **2012**, *134*, 6575−6578.
(183) Maitra, U.; Gupta, U.; De, M.; Datta, R.; Govindaraj, A.; Rao, C. N. R. Highly Effective Visible-Light Induced H_2 Generation by Single-Layer 1T-MoS_2 and a Nanocomposite of Few-Layer 2H-MoS_2 with Heavily Nitrogenated Graphene. *Angew. Chem., Int. Ed.* **2013**, *52*, 13057−13061.
(184) Meng, F.; Li, J.; Cushing, S. K.; Zhi, M.; Wu, N. Solar Hydrogen Generation by Nanoscale p−n Junction of p-type Molybdenum Disulfide/n-type Nitrogen-Doped Reduced Graphene Oxide. *J. Am. Chem. Soc.* **2013**, *135*, 10286−10289.
(185) Gupta, U.; Naidu, B. S.; Maitra, U.; Singh, A.; Shirodkar, S.; Waghmare, U. V.; Rao, C. N. R. Characterization of Few-Layer 1T-$MoSe_2$ and It Superior Photocatalytic Activity in the Hydrogen Evolution Reaction. *Appl. Phys. Lett. Mater.* **2014**, *2*, 092802.
(186) Ma, C.-B.; Qi, X.; Chen, B.; Bao, S.; Yin, Z.; Wu, X.-J.; Luo, Z.; Wei, J.; Zhang, H.-L.; Zhang, H. MoS_2 Nanoflower-Decorated Reduced Graphene Oxide Paper for High-Performance Hydrogen Evolution Reaction. *Nanoscale* **2014**, *6*, 5624−5629.
(187) Zeng, Z.; Tan, C.; Huang, X.; Bao, S.; Zhang, H. Growth of noble metal Nanoparticles on Single-Layer TiS_2 and TaS_2 Nanosheets for Hydrogen Evolution Reaction. *Energy Environ. Sci.* **2014**, *7*, 797−803.
(188) Chen, J.; Wu, X.-J.; Yin, L.; Li, B.; Hong, X.; Fan, Z.; Chen, B.; Xue, C.; Zhang, H. One-pot Synthesis of CdS Nanocrystals Hybridized with Single-Layer Transition-Metal Dichalcogenide Nanosheets for Efficient Photocatalytic Hydrogen Evolution. *Angew. Chem., Int. Ed.* **2015**, *54*, 1210−1214.
(189) Mou, Z.; Dong, Y.; Li, S.; Du, Y.; Wang, X.; Yang, P.; Wang, S.; Eosin, Y. Functionalized Graphene for Photocatalytic Hydrogen Production from Water. *Int. J. Hydrogen Energy* **2011**, *36*, 8885−8893.
(190) Sobczynski, A. Molybdenum Disulfide as a Hydrogen Evolution Catalyst for Water Photodecomposition on Semiconductors. *J. Catal.* **1991**, *131*, 156−166.
(191) Kanda, S.; Akita, T.; Fujishima, M.; Tada, H. Facile Synthesis and Catalytic Activity of MoS_2/TiO_2 by a Photodeposition-Based Technique and Its Oxidized Derivative MoO_3/TiO_2 with a Unique Photochromism. *J. Colloid Interface Sci.* **2011**, *354*, 607−610.
(192) Djamil, J.; Segler, S. A.; Dabrowski, A.; Bensch, W.; Lotnyk, A.; Schurmann, U.; Kienle, L.; Hansen, S.; Beweries, T. The Influence of Carbon Content on the Structure and Properties of MoS_xC_y Photocatalysts for Light-Driven Hydrogen Generation. *Dalton Trans.* **2013**, *42*, 1287−1292.
(193) Gupta, U.; Rao, B. G.; Maitra, U.; Prasad, B. E.; Rao, C. N. R. Visible-Light-Induced Generation of H_2 by Nanocomposites of Few-Layer TiS_2 and TaS_2 with CdS Nanoparticles. *Chem.—Asian J.* **2014**, *9*, 1311−1315.
(194) Song, P.; Zhang, X.; Sun, M.; Cui, X.; Lin, Y. Graphene Oxide Modified TiO_2 Nanotube Arrays: Enhanced Visible Light Photoelectrochemical Properties. *Nanoscale* **2012**, *4*, 1800−1804.
(195) Lin, Y.-G.; Lin, C.-K.; Miller, J. T.; Hsu, Y.-K.; Chen, Y.-C.; Chen, L.-C.; Chen, K.-H. Photochemically Active Reduced Graphene Oxide with Controllable Oxidation level. *RSC Adv.* **2012**, *2*, 11258−11262.
(196) Yavari, F.; Koratkar, N. Graphene-Based Chemical Sensors. *J. Phys. Chem. Lett.* **2012**, *3*, 1746−1753.
(197) He, Q.; Wu, S.; Yin, Z.; Zhang, H. Graphene-Based Electronic Sensors. *Chem. Sci.* **2012**, *3*, 1764−1772.
(198) Wu, S.; He, Q.; Tan, C.; Wang, Y.; Zhang, H. Graphene-Based Electrochemical Sensors. *Small* **2013**, *9*, 1160−1172.
(199) Novoselov, K. S.; Geim, A. K.; Morozov, S. V.; Jiang, D.; Zhang, Y.; Dubonos, S. V.; Grigorieva, I. V.; Firsov, A. A. Electric Field Effect in Atomically Thin Carbon Films. *Science* **2004**, *306*, 666−669.
(200) Yuan, W.; Shi, G. Graphene-Based Gas Sensors. *J. Mater. Chem. A* **2013**, *1*, 10078−10091.
(201) Wehling, T. O.; Katsnelson, M. I.; Lichtenstein, A. I. Adsorbates on Graphene: Impurity States and Electron Scattering. *Chem. Phys. Lett.* **2009**, *476*, 125−134.
(202) Schedin, F.; Geim, A. K.; Morozov, S. V.; Hill, E. W.; Blake, P.; Katsnelson, M. I.; Novoselov, K. S. Detection of Individual Gas Molecules Adsorbed on Graphene. *Nat. Mater.* **2007**, *6*, 652−655.
(203) Yoon, H. J.; Jun, D. H.; Yang, J. H.; Zhou, Z.; Yang, S. S.; Cheng, M. M.-C. Carbon Dioxide Gas Sensor Using a Graphene Sheet. *Sens. Actuators, B* **2011**, *157*, 310−313.
(204) Hwang, S.; Lim, J.; Park, H. G.; Kim, W. K.; Kim, D.-H.; Song, I. S.; Kim, J. H.; Lee, S.; Woo, D. H.; Chan Jun, S. Chemical Vapor

DOI: 10.1021/am509096x
ACS Appl. Mater. Interfaces 2015, 7, 7809−7832

Sensing Properties of Graphene Based on Geometrical Evaluation. *Curr. Appl. Phys.* **2012**, *12*, 1017−1022.
(205) Hugo, E. R.; Prasoon, J.; Awnish, K. G.; Humberto, R. G.; Milton, W. C.; Srinivas, A. T.; Peter, C. E. Adsorption of Ammonia on Graphene. *Nanotechnology* **2009**, *20*, 245501.
(206) Rumyantsev, S.; Liu, G.; Shur, M. S.; Potyrailo, R. A.; Balandin, A. A. Selective Gas Sensing with a Single Pristine Graphene Transistor. *Nano Lett.* **2012**, *12*, 2294−2298.
(207) Chen, C. W.; Hung, S. C.; Yang, M. D.; Yeh, C. W.; Wu, C. H.; Chi, G. C.; Ren, F.; Pearton, S. J. Oxygen Sensors Made by Monolayer Graphene Under Room Temperature. *Appl. Phys. Lett.* **2011**, *99*, 243502.
(208) Yu, K.; Wang, P.; Lu, G.; Chen, K.-H.; Bo, Z.; Chen, J. Patterning Vertically Oriented Graphene Sheets for Nanodevice Applications. *J. Phys. Chem. Lett.* **2011**, *2*, 537−542.
(209) Chen, G.; Paronyan, T. M.; Harutyunyan, A. R. Sub-ppt Gas Detection with Pristine Graphene. *Appl. Phys. Lett.* **2012**, *101*, 243502.
(210) Ghosh, A.; Late, D. J.; Panchakarla, L. S.; Govindaraj, A.; Rao, C. N. R. NO_2 and Humidity Sensing Characteristics of Few-Layer Graphenes. *J. Exp. Nanosci.* **2009**, *4*, 313−322.
(211) Bi, H.; Yin, K.; Xie, X.; Ji, J.; Wan, S.; Sun, L.; Terrones, M.; Dresselhaus, M. S. Ultrahigh Humidity Sensitivity of Graphene Oxide. *Sci. Rep.* **2013**, *3*.
(212) Yuan, W.; Liu, A.; Huang, L.; Li, C.; Shi, G. High-Performance NO_2 Sensors Based on Chemically Modified Graphene. *Adv. Mater.* **2013**, *25*, 766−771.
(213) Zhou, M.; Zhai, Y.; Dong, S. Electrochemical Sensing and Biosensing Platform Based on Chemically Reduced Graphene Oxide. *Anal. Chem.* **2009**, *81*, 5603−5613.
(214) Shao, Y.; Wang, J.; Wu, H.; Liu, J.; Aksay, I. A.; Lin, Y. Graphene Based Electrochemical Sensors and Biosensors: A Review. *Electroanalysis* **2010**, *22*, 1027−1036.
(215) Li, H.; Wu, J.; Qi, X.; He, Q.; Liusman, C.; Lu, G.; Zhou, X.; Zhang, H. Graphene Oxide Scrolls on Hydrophobic Substrates Fabricated by Molecular Combing and Their Application in Gas Sensing. *Small* **2013**, *9*, 382−386.
(216) He, Q.; Wu, S.; Gao, S.; Cao, X.; Yin, Z.; Li, H.; Chen, P.; Zhang, H. Transparent, Flexible, All-Reduced Graphene Oxide Thin Film Transistors. *ACS Nano* **2011**, *5*, 5038−5044.
(217) Sudibya, H. G.; He, Q.; Zhang, H.; Chen, P. Electrical Detection of Metal Ions Using Field-Effect Transistors Based on Micropatterned Reduced Graphene Oxide Films. *ACS Nano* **2011**, *5*, 1990−1994.
(218) He, Q.; Sudibya, H. G.; Yin, Z.; Wu, S.; Li, H.; Boey, F.; Huang, W.; Chen, P.; Zhang, H. Centimeter-Long and Large-Scale Micropatterns of Reduced Graphene Oxide Films: Fabrication and Sensing Applications. *ACS Nano* **2010**, *4*, 3201−3208.
(219) Zhan, Y.; Liu, Z.; Najmaei, S.; Ajayan, P. M.; Lou, J. Large-Area Vapor-Phase Growth and Characterization of MoS_2 Atomic Layers on a SiO_2 Substrate. *Small* **2012**, *8*, 966−971.
(220) Dey, S.; Matte, H. S. S. R.; Shirodkar, S. N.; Waghmare, U. V.; Rao, C. N. R. Charge-Transfer Interaction between Few-Layer MoS_2 and Tetrathiafulvalene. *Chem.—Asian J.* **2013**, *8*, 1780−1784.
(221) Perkins, F. K.; Friedman, A. L.; Cobas, E.; Campbell, P. M.; Jernigan, G. G.; Jonker, B. T. Chemical Vapor Sensing with Monolayer MoS_2. *Nano Lett.* **2013**, *13*, 668−673.
(222) Li, H.; Wu, J.; Yin, Z.; Zhang, H. Preparation and Applications of Mechanically Exfoliated Single-Layer and Multilayer MoS_2 and WSe_2 Nanosheets. *Acc. Chem. Res.* **2014**, *47*, 1067−1075.
(223) Late, D. J.; Huang, Y.-K.; Liu, B.; Acharya, J.; Shirodkar, S. N.; Luo, J.; Yan, A.; Charles, D.; Waghmare, U. V.; Dravid, V. P.; Rao, C. N. R. Sensing Behavior of Atomically Thin-Layered MoS2 Transistors. *ACS Nano* **2013**, *7*, 4879−4891.
(224) Wu, S.; Zeng, Z.; He, Q.; Wang, Z.; Wang, S. J.; Du, Y.; Yin, Z.; Sun, X.; Chen, W.; Zhang, H. Electrochemically Reduced Single-Layer MoS_2 Nanosheets: Characterization, Properties, and Sensing Applications. *Small* **2012**, *8*, 2264−2270.
(225) Zhu, C.; Zeng, Z.; Li, H.; Li, F.; Fan, C.; Zhang, H. Single-Layer MoS_2-Based Nanoprobes for Homogeneous Detection of Biomolecules. *J. Am. Chem. Soc.* **2013**, *135*, 5998−6001.
(226) Zhang, Y.; Zheng, B.; Zhu, C.; Zhang, X.; Tan, C.; Li, H.; Chen, B.; Yang, J.; Chen, J.; Huang, Y.; Wang, L.; Zhang, H. Single-Layer Transition Metal Dichalcogenide Nanosheet-Based Nanosensors for Rapid, Sensitive, and Multiplexed Detection of DNA. *Adv. Mater.* **2015**, *27*, 935−939.
(227) Li, H.; Yin, Z.; He, Q.; Li, H.; Huang, X.; Lu, G.; Fam, D. W. H.; Tok, A. I. Y.; Zhang, Q.; Zhang, H. Fabrication of Single- and Multilayer MoS_2 Film-Based Field-Effect Transistors for Sensing NO at Room Temperature. *Small* **2012**, *8*, 63−67.
(228) Paul, R. K.; Badhulika, S.; Saucedo, N. M.; Mulchandani, A. Graphene Nanomesh As Highly Sensitive Chemiresistor Gas Sensor. *Anal. Chem.* **2012**, *84*, 8171−8178.
(229) Wang, F.; Zhang, Y.; Tian, C.; Girit, C.; Zettl, A.; Crommie, M.; Shen, Y. R. Gate-Variable Optical Transitions in Graphene. *Science* **2008**, *320*, 206−209.
(230) Nair, R. R.; Blake, P.; Grigorenko, A. N.; Novoselov, K. S.; Booth, T. J.; Stauber, T.; Peres, N. M. R.; Geim, A. K. Fine Structure Constant Defines Visual Transparency of Graphene. *Science* **2008**, *320*, 1308.
(231) Xia, F.; Mueller, T.; Lin, Y.-m.; Valdes-Garcia, A.; Avouris, P. Ultrafast Graphene Photodetector. *Nat. Nanotechnol.* **2009**, *4*, 839−843.
(232) Mueller, T.; Xia, F.; Avouris, P. Graphene Photodetectors for High-Speed Optical Communications. *Nat. Photon* **2010**, *4*, 297−301.
(233) Chitara, B.; Panchakarla, L. S.; Krupanidhi, S. B.; Rao, C. N. R. Infrared Photodetectors Based on Reduced Graphene Oxide and Graphene Nanoribbons. *Adv. Mater.* **2011**, *23*, 5419−5424.
(234) Chitara, B.; Krupanidhi, S. B.; Rao, C. N. R. Solution Processed Reduced Graphene Oxide Ultraviolet Detector. *Appl. Phys. Lett.* **2011**, *99*, 113113−113114.
(235) Lee, H. S.; Min, S.-W.; Chang, Y.-G.; Park, M. K.; Nam, T.; Kim, H.; Kim, J. H.; Ryu, S.; Im, S. MoS_2 Nanosheet Phototransistors with Thickness-Modulated Optical Energy Gap. *Nano Lett.* **2012**, *12*, 3695−3700.
(236) Chou, S. S.; Kaehr, B.; Kim, J.; Foley, B. M.; De, M.; Hopkins, P. E.; Huang, J.; Brinker, C. J.; Dravid, V. P. Chemically Exfoliated MoS_2 as Near-Infrared Photothermal Agents. *Angew. Chem., Int. Ed.* **2013**, *52*, 4160−4164.
(237) Rao, C. N. R.; Matte, H. S. S. R.; Subrahmanyam, K. S. Synthesis and Selected Properties of Graphene and Graphene Mimics. *Acc. Chem. Res.* **2013**, *46*, 149−159.
(238) Yin, Z.; Li, H.; Li, H.; Jiang, L.; Shi, Y.; Sun, Y.; Lu, G.; Zhang, Q.; Chen, X.; Zhang, H. Single-Layer MoS_2 Phototransistors. *ACS Nano* **2012**, *6*, 74−80.
(239) Lopez-Sanchez, O.; Lembke, D.; Kayci, M.; Radenovic, A.; Kis, A. Ultrasensitive Photodetectors Based on Monolayer MoS_2. *Nat. Nanotechnol.* **2013**, *8*, 497−501.
(240) Tsai, D.-S.; Liu, K.-K.; Lien, D.-H.; Tsai, M.-L.; Kang, C.-F.; Lin, C.-A.; Li, L.-J.; He, J.-H. Few-Layer MoS_2 with High Broadband Photogain and Fast Optical Switching for Use in Harsh Environments. *ACS Nano* **2013**, *7*, 3905−3911.
(241) Schwierz, F. Graphene Transistors. *Nat. Nanotechnol.* **2010**, *5*, 487−496.
(242) Radisavljevic, B.; Radenovic, A.; Brivio, J.; Giacometti, V.; Kis, A. Single-Layer MoS_2 Transistors. *Nat. Nanotechnol.* **2011**, *6*, 147−150.
(243) Zeng, H.; Dai, J.; Yao, W.; Xiao, D.; Cui, X. Valley Polarization in MoS_2 Monolayers by Optical Pumping. *Nat. Nanotechnol.* **2012**, *7*, 490−493.
(244) Mak, K. F.; He, K.; Lee, C.; Lee, G. H.; Hone, J.; Heinz, T. F.; Shan, J. Tightly Bound Trions in Monolayer MoS_2. *Nat. Mater.* **2013**, *12*, 207−211.

DOI: 10.1021/am509096x
ACS Appl. Mater. Interfaces 2015, 7, 7809−7832